Investigating the Autocatalytic Self-Assembly of Keggin-based Polyoxometalate Clusters

David Lockey

A dissertation submitted to the University of Glasgow for the degree of Master of Science by Research (MScR)

School of Chemistry

College of Science and Engineering

July 2021

“A man with new ideas is a madman, until his ideas triumph” – Marcelo Bielsa

Acknowledgments

This project was undertaken between October 2019 and June 2021 within the school of Chemistry at the University of Glasgow. The research was performed under the supervision of Professor Leroy Cronin. The following list is people I would like to express my gratitude to, as they have been invaluable in helping with this project.

Prof. Leroy Cronin for giving me time, guidance, and the opportunity to work in such a dynamic research group. The invaluable experience gained by working with such gifted people, the provision of resources to allow me to explore project ideas and goals and the experience gained in a wide range of techniques is something I will carry for the rest of my life. The discussion and planning of various ideas and experiments (no matter how crazy) will be of particular influence in allowing me to go forward within the world of chemistry.

Dr Haralampos Miras for his time, patience, and guidance in completing the work undertaken within this thesis. The many discussions we had regarding this project gave me valuable insight into how the world of inorganic chemistry behaves and I am excited to see what he accomplishes in the future. This work would not have been possible without him.

Dr Nicola Bell for all the hard work she undertakes in not just being a great team leader but also a wonderful group coordinator. Her patience, guidance and helpful nudging along the way was critical in getting this work finished. Her knowledge of chemistry is second to none, something which has been particularly helpful, and I'm sure she will accomplish great things in the coming years.

Dr Deliang Long for also being a fantastic team leader and for all of his help and insight over the last three years. His vast knowledge within the world of POMs and inorganic chemistry were vital in helping me to gain a deeper understanding of this field. Furthermore, his expertise in X-ray crystallography has helped me dramatically over the years and have been essential for the completion of this work.

While the above people have been instrumental in allowing the completion of this thesis, there are many others that I would also like to extend my gratitude towards.

First of all, I would like to thank **Dr Cole Mathis** for his work on the computational part of this project, I always enjoyed his unique presentations and I'm sure he will go on to accomplish great things. **Eduard Garrido Ribo** for not only providing useful discussions on POMs but for also being a great friend and lab buddy. I wish him the best of luck in the future and hope he remembers to look to the east at dawn. **Tze-Kiat (Marcus) Ng** for helping to keep me sane during the last stretch of my thesis. His ability to distract from me from doing any work is unrivalled and I wish him the very best for the rest of his PhD and for the future (especially in crypto). **Dr Edward Lee** for all his discussions on science, life, video games and everything else in between. He made me feel welcome right from the very start of my time in the Cronin group as an undergraduate and I owe him a lot for all his help during my time in the group. I'm sure he has a wonderful career ahead of him. I would also like to thank members of the group who work to ensure it runs as smoothly as possible and have been of insurmountable help. **Sebastian Manzano** for being a great friend and taking up way too much of my time to talk all things football. Vamos Leeds Carajo. **Yibin Jiang** for all of the laughs he has given me, as well as insightful scientific discussions. He may just about be the smartest person I've ever met and I'm sure he is destined for great things within chemistry. **Amanda McGarvey** for being my go-to person with any problems I had and who without, the group would almost certainly crumble. **Jim McIver** for keeping everything running smoothly and for always being willing to help with even the most trivial of issues. **Dr Diana Castro** for always being happy to help with anything and everything and for her help with the mass spectrometry involved in this thesis.

A further thanks is to be extended to past and present members of the clusters team, who have all provided help and guidance throughout my time within the group: **Dr. Robert Pow, Dr. Weimin Xuan, Dr. Nancy Watfa, Zoe Sinclair, Dr. Pablo Martinez Bulit, Dr. Shan She. Dr. Tingting Zhao, Daniel Kowalski, Dr Yousef Abul-Haija, Dr. Laia Vila-Nadal, Dr. Balamurugan Kandasamy, Dr. Naomi Johnson, Manuel Kupper,** and anybody else I am forgetting.

Many thanks to office mates who helped create a pleasant work environment: **Andrius Bubliauskas, Dr. Simon Rohrbach** and **Dr Wenduan Hou** and anybody else I am forgetting.

Finally, I would not have finished this thesis without the continued help and support from my family and friends. Their never-ending encouragement makes me always want to push further and accomplish what I can. This thesis wouldn't have been possible without them. Specifically, I would like to give the biggest thanks to one person in particular: **Rebecca Baird.** Without her, none of this would be possible. She has continued to believe in me and continuously makes me strive to be the best version of myself. I cannot even begin express the gratitude and love I have for her. This thesis is for her.

Table of Contents

Abstract 8
1 Introduction 9
1.1 Polyoxometalates 9
1.1.1 Early History 9
1.1.2 Polyoxometalate Nomenclature 11
1.1.3 Polyoxometalate Bonding 11
1.1.4 Polyoxometalate Synthesis 13
1.2 Classical Polyoxometalates 14
1.2.1 Lindqvist 15
1.2.2 Keggin 15
1.2.3 Anderson-Evans 16
1.2.4 Wells-Dawson 17
1.2.5 Other Small POMs 18
1.3 Large Molybdenum Clusters 20
1.4 Mechanisms and Self assembly 25
1.5 Introduction into autocatalysis 27
1.5.1 General mechanism 27
1.5.2 Direct Autocatalysis 27
1.5.4 Network Autocatalyses 28
1.5.4.1 Indirect Autocatalysis 29
1.5.4.2 Collective Autocatalysis 29
1.6 Monitoring Autocatalysis 29
1.7 Examples of autocatalytic sets 33
1.7.1 Organic reactions – Chemical Clocks: 33
1.7.2 Formose Reaction 34
1.7.3 DNA Replication 36
1.7.4 MOFs/POMs: 36
2 Aims and Abstract 39
3 Investigation of Autocatalysis in Keggin-based POM Clusters 40
3.1 Introduction into Autocatalysis and Previous Experiments 40
3.2 Novel Experiments and Data 44
3.2.1 Initial Reaction 44
3.2.2 Temperature Variation Experiments for $AsMo_{12}$ 45
3.2.3 Seeding Experiments for $AsMo_{12}$ 46

3.2.4 Temperature Variation Experiments for $SiMo_{12}$ 48
3.2.5 Seeding Experiments for $SiMo_{12}$ 49
3.2.6 Concentration Variation Experiments 51
3.2.7 Mass Spectrometry Experiments 52
3.3 Computational Model 55
3.4 Discussion and Conclusion 57
3.5 Future Work 58
4 Improving the Synthesis of Mo_{368} 59
4.1 The Architecture of Mo_{368} 59
4.2 The Synthesis of Mo_{368} 61
4.3 Conclusions and Future Work 70
5 Experimental 72
5.1 Materials 72
5.2 Instrumental 72
5.2.1 UV-Vis Spectroscopy 72
5.2.2 Single Crystal X-Ray Diffraction 72
5.2.3 pH Measurements 72
5.2.4 Mass Spectrometry Monitoring 72
5.3 Computational Model Details 73
5.4 Monitoring of $\{AsMo_{12}\}$ formation 75
5.5 Monitoring of $\{SiMo_{12}\}$ formation 75
5.6 Preparation of $\{AsMo_{12}\}$ Seed 75
5.7 Preparation of $\{SiMo_{12}\}$ Seed 75
6 References 77

Abstract

Many areas of chemistry strive towards the directed synthesis of complex molecules. Polyoxometalates (POMs) are discrete metal oxide clusters that span a wide area of chemistry and are often topologically complex or interesting. They can be formed from many different atom types and in many different reaction conditions and can include a range of inorganic and organic complexes within their structures. Their variable structures and functions have led to use in many areas of chemistry, most notably catalysis.

The way that the formation of discrete clusters is achieved is still largely unknown and is often called “self-assembly”. An investigation into the kinetics of the Keggin type POM was looked at using a UV/Vis detection-based system in order to find the underlying kinetics of the reaction. This revealed an underlying autocatalytic formation system in which the Keggin catalyzes its own formation, providing vital further insight into how these clusters are formed in situ.

Also, the synthesis of the largest known POM, the Mo_{368}, was looked at. Notoriously difficult to synthesize based on literature conditions, the goal was to improve the synthesis in order to obtain high quality single crystals of the cluster. A better understanding of the synthesis of the largest POM cluster would allow for further clarity into the exact conditions and could provide insight into the sort of reaction equilibria needed to form even larger structures. This was achieved by employing a robotic liquid handling platform for high

accuracy synthesis. Specific areas of synthesis were targeted, and the reaction conditions changed depending on the results of previous reaction runs.

1 Introduction

1.1 Polyoxometalates

Polyoxometalates can be described as discrete inorganic metal oxide clusters known as polyoxoanions or polyanions. They are can be comprised of a wide range of group V and group VI transition metals, although the metals most commonly found in their composition are tungsten, molybdenum and vanadium. They can either be comprised of only one metal type, which forms species called isopolyoxometalates, or can include a mixture of different metal species, forming heteropolyoxometalates. The interest in POMs has grown vastly over the years, which can be centered around two important features: Firstly, POMs have a very wide structural diversity that results in structures with atom totals ranging from tens to thousands. As a consequence of this, not only does this raise questions as to how complex chemical systems behave and how simple metal salt solutions can come together to offer said structural diversity, but it also pushes inorganic chemistry into a domain that is comparable to that of organic macromolecules and proteins. Secondly, the vast number of different elements of the periodic table that can be incorporated into these structures offers an insight into fundamental chemical questions about bonding and matter organisation in solution, whilst also exploring the potential access to multiple physical and chemical properties. POMs already have a wide range of potential properties, which extends to medicine[1], magnetism[2,3], catalysis[4] and material design[5,6].

1.1.1 Early History

Polyoxometalates can date as far back as 1793 when Scheele discovered what is now known to be the first example of a reduced molybdenum cluster known as molybdenum blues, when he was investigating reduced molybdenum salts.[7] The next important step in POM history came in 1826 when Swedish chemist Jöns Jacob Berzelius reported the formation of a yellow precipitate when reacting phosphoric acid and ammonium molybdate.[8] This yellow precipitate is the first isolated Keggin-type structure, $(NH_4)[PMo_{12}O_{40}]$. Many years later, in 1862, Swiss chemist Jean-Charles Galissard de Marignac reported the first accurate description of the elemental composition of POMs after his discovery of two Keggin analogues. These were the α- and β-isomers of silicotungstic acid ($H_4[W_{12}SiO_{40}]$, which he

correctly ascertained their composition via titrations.[9] Due to the absence of modern analytical techniques, mainly the unavailability of the powerful X-ray diffraction (XRD) tools used for structural characterisation that exist today, multiple theories arose surrounding the bonding and exact structural aspects of these early metal clusters. Many chemists in the early 20th century including Werner, Miolati and Pauling formed hypotheses around the most probable structures and bonding mechanisms that could be occurring. Italian chemist Arturo Miolati, together with German chemist Arthur Rosenheim, proposed the Miolati-Rosenheim theory in 1910. This theory was based on the hypothesis that these {XMo_{12}} structures were formed of six-coordinate octahedral heteroatoms from the parent acids by replacing their oxo ligands with MO_4^{2-} or $M_2O_7^{2-}$ ligands.[10] However, despite initial support for this theory, American chemist Linus Pauling put forward a different theory in 1929. His theory suggested that the heteroatom from the parent acid is instead in a tetrahedral environment surrounded by corner sharing MO_6 octahedra.[11] However, although his theory accurately described the basicity seen in tungsten and molybdenum Keggin (XM_{12}} and Dawson {X_2M_{18}} heteropolyoxometalates, it also resulted in the predicted structures being very electron rich due to the limitation of only corner shared metal addenda. This limitation was down to the thought that edge and face shared octahedral were considered unfeasible due to the large electronic charge.[11] When the further development of X-ray diffraction was available, British crystallographer James Keggin was finally able to accurately determine the structural composition of the {XM_{12}} Keggin, to which he is the namesake. This breakthrough confirmed aspects of Pauling's theory, mainly that the tetrahedral heteroatom is surrounded by MO_6 octahedra, but showed that the metal octahedra could be linked via corner and edge-sharing.[12] The structure in question was that of phosphotungstic acid ($H_3[PW_{12}O_{40}]$), which comprises of both corner and edge shared oxo ligands in its WO_6 octahedra.[13] A few years later, in 1937, Anderson predicted the structure of another very common polyoxometalate structure, that was later confirmed by Evans via X-ray crystallography. The exact structure found was that of $[TeMo_6O_{24}]^{6-}$ and comprises of a planar ring of MoO_6 octahedra in an edge shared configuration surrounding a central TeO_6 octahedra. This structure was named after both chemists and is known as the Anderson-Evans structure or, more commonly, the Anderson structure.[14,15] As the years have gone on, the further development surrounding the analysis and structural determination methods of polyoxometalates has allowed for increasingly larger structures to be determined. German chemist Achim Müller has been a leading name in the advancement of large polyoxometalates for many years, including the discovery of the wheel type Mo_{154}

structure,[16] the gigantic Keplerate-type Mo_{132}[17] and the largest POM known to date, the Mo_{368}, otherwise known as the "blue lemon" or "hedgehog".[18]

1.1.2 Polyoxometalate Nomenclature

Due to the large number of atoms, the multitude of structures and the high number of configurations and coordination environments involved, the nomenclature of POMs lacks conventional systematic rules that would be applied to something like organic systems. Jeannin and Fournier proposed a naming system for POMs that was adopted into IUPAC guidelines in order to remove potential structural ambiguities. This naming system first defines the axis of the highest rotational order and then begins labelling the metal atoms in a clockwise manner, starting at 12 o'clock. This also starts at the top of the structure and works its way down into the subsequent planes that the metal atoms lie in until the whole structure is assigned.[19] However, beyond small, low-nuclearity POMs, this nomenclature system is both tedious and extremely complex and so is very rarely put into practice. As a result of this, the formulae are instead often given in a shorthand version, encased in {}, which contain the most important aspects of the POM in question. This has historically been the number of metal atoms, framework oxygen atoms and any adjoined ligands, however in recent years many times POMs are simply referred by the number of metal atoms. Although this is a much more straightforward system, it also comes with the added hindrance of having no standardised rules, which can cause further confusion between researchers and it also means some structural details can be left out, such as the position of ligands or coordination sites, that would otherwise be distinguishable in the absence of a physical structure image. Further complications can also arise when the use of historical names is used, such as the Dawson, Anderson and Keggin structures, although this can sometimes be a helpful addition and allow researchers to have a reference point to compare new structures to. Throughout this thesis, historical names, and shorthand versions of strcutures will be used.

1.1.3 Polyoxometalate Bonding

Polyoxometalates can be broken down into three major components: heteroatoms, metal addenda and oxo ligands. Heteroatoms are found within the POM structure and are surrounded by the addenda. They are usually p-block elements such as P, Si, S and As but can also extend to other elements, so long as it is capable of bonding to at least three atoms. Heteroatoms in POMs can either be primary/central or secondary/peripheral and this is a further distinction to make when looking at POMs. A primary heteroatom is critical to the

formation of the POM and acts as the template in which the POM builds itself around. However, secondary heteroatoms can be removed without destroying the structure. These structures are known as *lacunary* POMs, as the cavity left behind is the *lacuna*. Another distinction that can be made regarding the heteroatoms in POMs splits them into two categories: isopolyoxometalates and heteropolyoxometalates. Isopolyoxometalates have the general formula of $[M_nO_y]^p$, whereas heteropolyoxometalates have the general formula of $[X_aM_nO_y]^p$, where M is the metal addenda, X is the heteroatom, p is the charge of the POM and $a<n$.[20]

The metal addenda are the main scaffold when it comes to the architecture of POM structures. The addenda have specific rules that were outlined by Baker in 1998: (1) Upon acidification, the coordination number of the metal can vary between 4 and 7, (2) possess a high positive charge, (3) they are one of the smallest ions capable of octahedral packing and (4) they are able to form terminal M=O bonds via dπ-pπ interactions.[21] Addenda are usually early transition metals, often in their highest oxidation states, with d^0 or d^1 electronic configurations, such as W^{VI}, Mo^{VI} and V^{V}.

Finally, the oxo ligands that bond to the metal addenda can also be broken down further into two categories: bridging and terminal. Bridging oxygen atoms are bound to two or more of the metal addenda, whereas the terminal oxygen atoms form a double bond with the metal atom and are found at the cluster edges. The oxygen atoms surrounding a metal centre form what is known as a polyhedra and is most commonly in an octahedral geometry (coordination number of 6), although can be a variety of structural motifs. The terminal oxygen atom that forms the double bond to the metal centre is essential in the formation and building of discrete, well defined clusters and is the reason why these clusters don't aggregate to form infinite structures, such as iron oxides.[22] The reason for this is due to the trans-influence that is observed and is a weakening of a metal-ligand bond due to the ligand in the relative trans position and occurs in octahedral geometries, although it is not exclusive to this. Specifically, it is caused because the two ligands in the trans positions share the same orbital of the central metal atom and so if these ligands have a difference in their ability to donate and accept electrons, their bonding stabilities will change. In the case of POMs, the terminal M=O oxo-ligand is a much better electron donor than the bridging oxygen to the central metal atom and so a shortening of this terminal M=O bond occurs, lengthening the opposite (or trans) bridging oxygen bond. This difference in bond lengths results in a cluster-wide polarisation throughout, with the inside of the cluster being more electron rich than the

outside. This means that the terminal M=O ligands are much less susceptible to protonation and the whole cluster becomes stabilised and can form discrete, well-defined architectures. Yet another classification of POMs can be made depending on the type and number of terminal oxygen bonds. Structures with octahedra containing only one M=O terminal ligands are Type I, structures with octahedra containing two terminal cis-oxo-ligands are Type II and structures that contain a mixture of both are Type III.[23]

The polymerisation of the small metal $\{MO_x\}$ (most commonly $\{MO_6\}$) building units is achieved through acid-mediated condensation reactions. The $\{MO_6\}$ octahedral building units are the basic building block of most POMs and can come together in three different ways – corner, edge, or face sharing. The continued building of octahedra in this way can occur as long as the Lipscomb Principle is followed.[24] This states that no metal atoms can contain three terminal oxygen atoms, although a small number of structures have been found that violate this rule.[25,26]

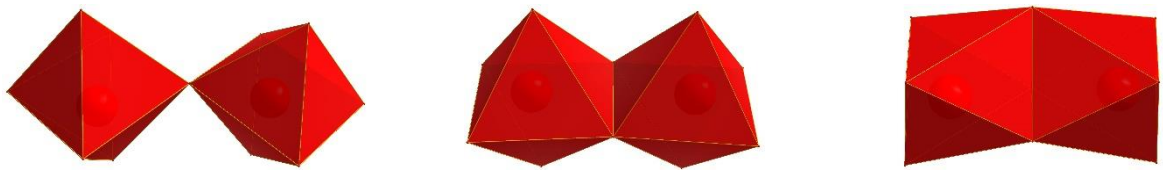

Figure 1 Polyhedral representation of metal addenda showing corner shared, edge shared and face shared respectively.

Polyoxometalate synthesis has evolved enormously over the course of many decades of research and as such can become complex and require the precise control of many synthetic variables, including temperature, pressure, pH, ionic strength, reaction concentration and the ratio of reagents. However, generally speaking, many polyoxometalates are synthesised via one pot reactions involving the specific metal oxides and any desired heteroatom under acidic conditions.[27] In addition to this, many other types of reagent can be used to form a multitude of different clusters, such as oxidants, reducing agents, organic ligands and lanthanides. This is also mainly done in aqueous media but many examples exist of POMs being synthesised in non-aqueous or mixed solvent environments, especially polar organic solvents such as acetonitrile or dichloromethane.[28–31]

Furthermore, although many POMs are easily made at room temperature, relatively recent advances have been made using highly elevated temperatures[32] and have even extended into

extreme pressures too by employing hydrothermal or solvothermal conditions.[33,34] This allows the reaction to proceed at conditions extremely far from equilibrium and obtains POMs that would otherwise not crystallise out if made at room temperature.

Another crucial part of the process regarding the synthesis of POMs is the crystallisation and subsequent purification and isolation. This is largely due to the fact that the most important aspect of characterising a cluster is arguably X-ray crystallography and so well defined, large crystals are often needed. A number of conditions can affect this process including temperature, location, air humidity and even the shape of the flask that the mother liquor is left in to crystallise. Furthermore, this adds in another complication of charge balancing the cations to allow for crystallisation and can be a wide range of elements and molecules including alkali metals, such as Na and K, and amines such as tetrabutylammonium.

The organisation of small building blocks via aggregation into large, discrete clusters that occurs during POM synthesis is said to occur via a self-assembly process. The exact mechanisms that occur during this process still aren't fully understood although is said to proceed via template mediated and molecular recognition processes.[35] Recent work in the Cronin group has found that one of the most well-known POMs, the $\{Mo_{154}\}$, is formed by an autocatalytic network where small inorganic replicators occur and catalyse their own formation and template the assembly of the giant POM structure. This is even more interesting as it explains why very specific building blocks are found in these systems in a solution that could in principle form thousands of combinatorial structures.[36] The work carried out in this thesis is a continuation of this and will explore the possible autocatalytic networks in other polyoxometalates.

1.2 Classical Polyoxometalates

Although there is an unprecedented amount of POM structures today, there are a number of common archetypal architectures that frequently occur due to their high stability and reproducibility. These structures can be formed from a wide range of metal addenda and heteroatoms and are often found as sub-structures for larger polyoxometalates or even as starting materials in large POM synthesis. The next section will introduce a multitude of these classical POM examples.

1.2.1 Lindqvist

The Lindqvist was first reported by Swedish chemist Ingvar Lindqvist in 1950. It is the smallest and most simple of the classical POM and has the general formula of $[M_6O_{19}]^{n-}$. The structure contains six isopolyoxometalate units in an octahedral formation, giving an O_h symmetry, with all of the terminal M=O ligands forming the outer corners of the structure, which also makes it a Type I polyoxometalate. The metal addenda within the structure can be formed from a variety of elements, such as Mo[37,38], W[39], Nb[40] and Ta[41]. The Lindqvist structure can also be used as a building block in the synthesis of larger structures.[42]

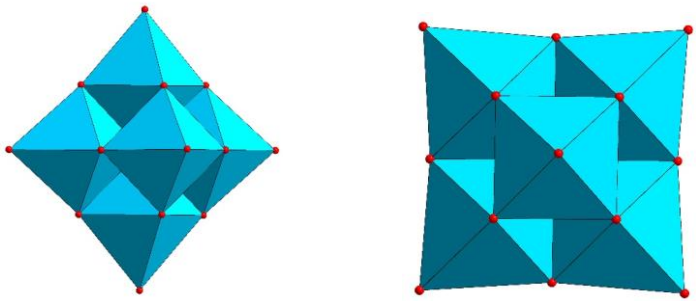

Figure 2 Polyhedral representation of the Lindqvist POM showing side view and top-down view. (Colour scheme: Metal octahedra = blue, oxygen = red)

1.2.2 Keggin

As described previously, the Keggin structure was fully identified in 1933 by British crystallographer James Keggin and was made possible by the advancement of X-ray crystallography techniques. The general formula is $[XM_{12}O_{40}]^{n-}$, where X is the heteroatom (common examples are P, Si, S, As, Si)[43] and M is the metal addenda atoms that assemble around the heteroatom (most commonly W and Mo). The structure itself comprises of four $\{M_3O_{13}\}$ triads, composed of octahedral metal atoms, surrounding a central tetrahedral heteroatom. The octahedra in the metal triads are connected via edge-shared oxygen but triads are connected to each other via corner shared oxygen ligands. As each individual metal octahedra only has one terminal M=O bond, the Keggin is a Type I POM. In total, 5 different basic Keggin structures exist, and this depends on the orientation of each triad relative to one another. The original structure is labelled as the α-Keggin and a 60° rotation of individual triads leads to the β[44], γ[45], δ[46] and ε[47] isomers respectively. The Keggin has

structure has also been found made entirely from unusual metal addenda, such as Al[48] or Fe[49], although these are not true POMs and many cases with unique metal addenda such as these commonly have to be held together with the assistance of organic ligands. The Keggin structure is also very stable and can undergo reversible reduction up to 24 electrons without disintegration[50], although most commonly reduced Keggins are only reduced by one or two electrons and are extremely stable, which will be the subject of work later in this thesis. The Keggin structure has found the most use in industry and has applications in catalysis.[51,52]

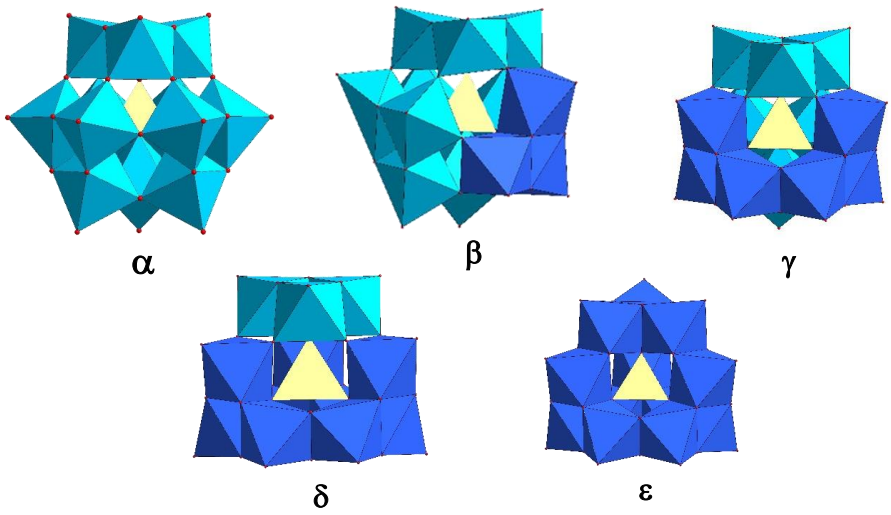

Figure 3 Polyhedral representation of Keggin structures, showing 5 different isomers. (Colour scheme: heteroatom X = yellow, metal octahedra = blue, oxygen = red)

1.2.3 Anderson-Evans

The Anderson-Evans structure has the general formula of $[XM_6O_{24}]^{n-}$ and was first speculated by Anderson in 1937 but it wasn't until 1948 that Evans finally determined the full structure.[15,53] The structure can be described as a hexagonal ring of edge shared octahedral addenda surrounding a central heteroatom octahedron. Interestingly, the central heteroatom can be a multitude of different elements, including first row transition metals[54], various P-block elements[55] and can also be another metal addenda atom (such as W, V or Mo). The Anderson-Evans can adopt one of two isomeric configurations depending on whether or not the central atom is another metal addendum or not. The two isomers are labelled as α and β and as well as having slightly different elemental compositions, they also have different spacial geometries too. The β-isomer has a characteristic planer geometry but when the central atom is another addendum, it becomes the α-isomer and loses its planarity and adopts a bent geometry.

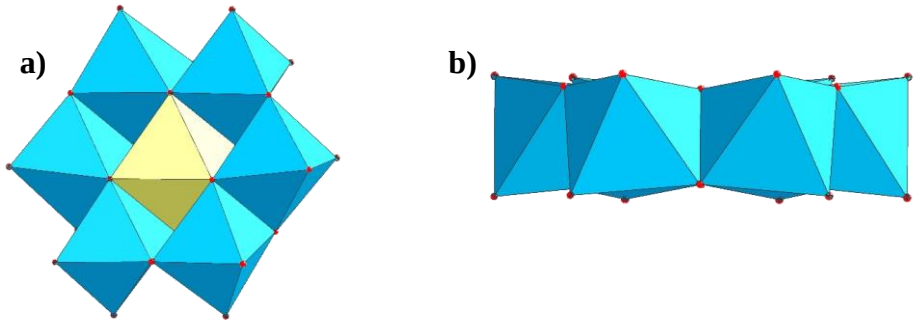

Figure 4 Polyhedral representation of Anderson-Evans structure showing a) top-down and b) side-on (Colour scheme: heteroatom X = yellow, metal octahedra = blue, oxygen = red)

1.2.4 Wells-Dawson

The Wells-Dawson structure has the general formula $[X_2M_{18}O_{62}]^{n-}$ and was first synthesized by Kehrmann in 1894 but wasn't structurally determined by Dawson until 1953, with Wells separately describing the structure.[56] The structure can be depicted as two Keggin units, each with a triad of metal addenda removed, sandwiched together. It can be further broken down as two belt regions, comprising of $\{M_6O_{18}\}$, and two capping regions, comprised of $\{M_3O_{13}\}$ units (the normal triad found in a Keggin). As is the case with the Keggin structure, the capping triads can be rotated 60° and results in the Wells-Dawson having three distinct isomeric groups of α, β and γ. Interestingly, the stabilities of these clusters change depending on the central heteroatoms that are inside the structures. Computational studies carried out in 2011 determined that when the central heteroatom is phosphorous, the stability follows a decreasing order of $\alpha > \beta > \gamma$.[57] However, when the heteroatom is changed to arsenic, the stability follows a decreasing order of $\gamma > \alpha > \beta$.[58] Much like Keggins, Wells-Dawson structures have found an application in catalysis.[59,60]

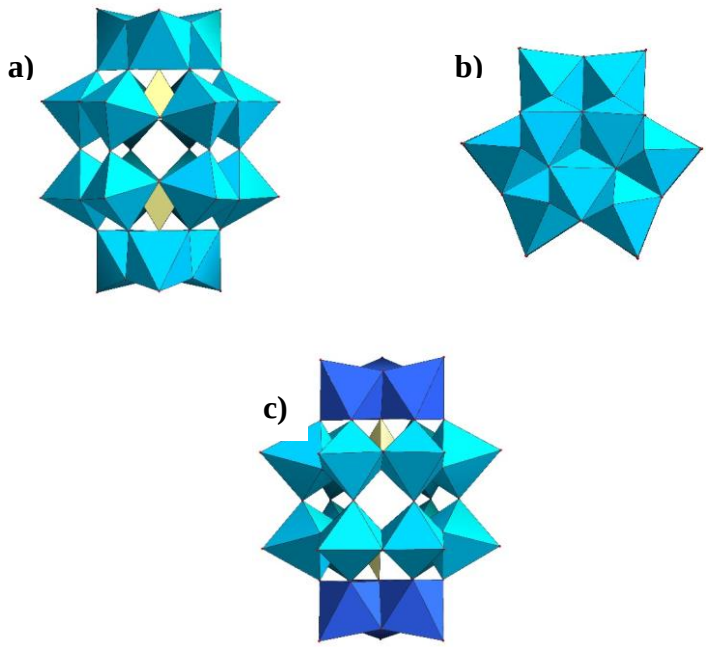

Figure 5 Polyhedral representation of Wells-Dawson structure. a) showing the side on, b) showing top-down and c) highlighting two $\{M_3O_{13}\}$ triads (dark blue) capping two central $\{M_6O_{18}\}$ belt regions (light blue) (Colour scheme: heteroatom X = yellow, metal octahedra = blue, oxygen = red)

1.2.5 Other Small POMs

Although the most common POMs have already been described, there are also a number of other small POMs with interesting architectures. One of these structures is known as the Weakley-Yamase structure and has the general formula of $[XM_{10}O_{36}]^{n-}$. This structure was important as it was the first example of a POM outside of the Keggin that contains a lanthanide heteroatom.[61] The structure can be described as a central heteroatom capped by two $\{M_5O_{18}\}$ units, in a sandwich like manner. Much like previous examples, the Weakley-Yamase structure has found a use in industry as a catalyst, specifically in the use of alcohol oxidation and alkene epoxidation.[62]

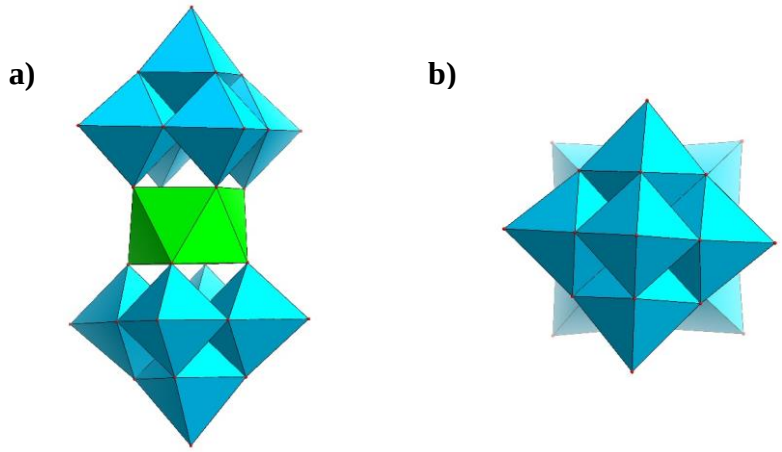

Figure 6 Polyhedral representation of Weakley-Yamase structure. a) side on and b) top-down view. (Colour scheme: Metal octahedra = blue, heteroatom X = green).

In 1973, Swedish crystallographer Rolf Strandberg isolated and solved a cluster with the general formula $[X_2M_5O_{23}]^{n-}$, to which he has become the namesake in the Strandberg POM.[63] The structure can be described as a ring of 5 $\{MO_6\}$ octahedral subunits, which are all edge shared except for one, resulting in a sort of distorted ring shape. It is also capped at both ends by tetrahedral $\{XO_4\}$ heteroatom subunits via three bridging oxo-ligands. The heteroatoms are usually phosphorous, although other structures with sulfur[64] and selenium[65] have also been identified.

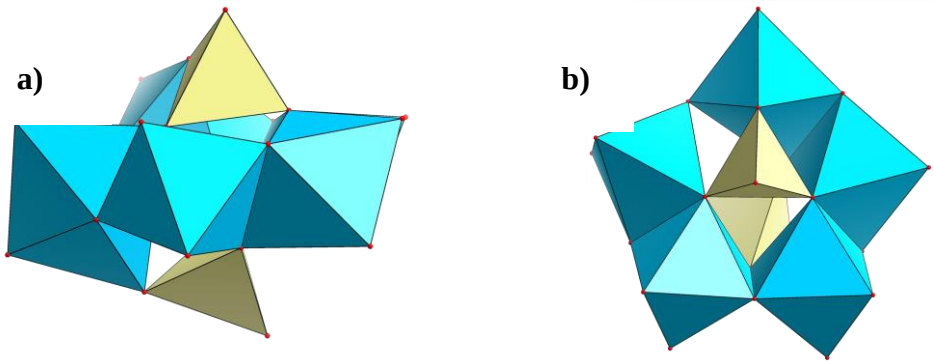

Figure 7 Polyhedral representation of Strandberg structure. a) side on and b) top-down view. (Colour scheme: heteroatom X = yellow, metal octahedra = blue, oxygen = red)

The Dexter-Silverton structure was isolated and solved in 1968 by David D. Dexter and J.V. Silverton and was the first POM that displayed face-sharing octahedra of the metal addenda. The structure can be described as twelve $\{MO_6\}$ metal octahedra surrounding a central heteroatom that is a twelve coordinate icosahedron and can be Ce^{IV}, Zr^{IV} or Th^{VI}.[66]

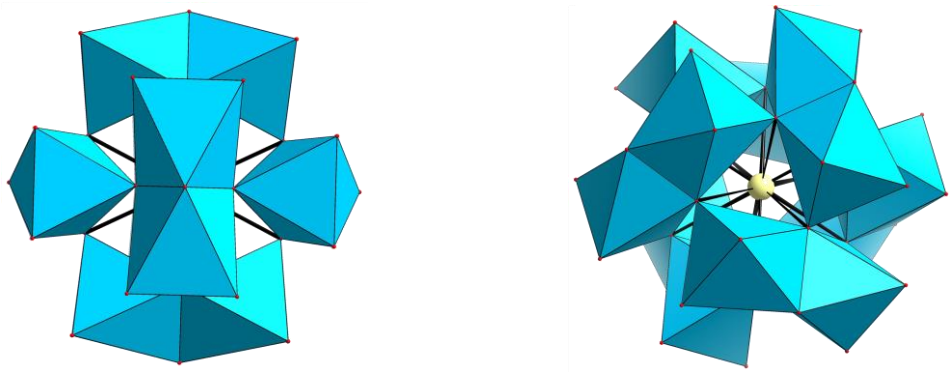

Figure 8 Polyhedral and ball-and-stick representation of the Dexter-Silverton POM (Colour scheme: heteroatom X = yellow, metal octahedra = blue, oxygen = red)

The Allman-Waugh was isolated and solved in 1954[67] and has the general formula of $[XM_9O_{32}]^{n-}$. This structure is interesting as it is one of the first polyoxometalates to be inherently chiral with respect to the metal atoms and usually is obtained in a racemic mixture. However, enantiopure crystals can be obtained depending on what cation is used to crystalize the POM and can also be separated by hand, although this process is often tedious.[68] It can be obtained from the previously described Anderson-Evans structure, as use as a precursor, where another $\{M_3O_8\}$ unit is added.

1.3 Large Molybdenum Clusters

Previously in this thesis, POMs were broken down into isopolyoxometalates and heteropolyoxometalates. However, a third major family of polyoxometalates exists in the form of large, reduced molybdenum clusters. These can be placed into two distinct groups known as molybdenum blues, largely composed of wheel-type structures, and molybdenum browns, largely composed of spherical structures. Despite extreme differences in these two types of structures, they are composed of similar common building blocks. These building blocks are referred to only by their number of metal atoms but are representative of

octahedral polyhedra and are enclosed in {} brackets. They are the $\{Mo_1\}$ unit, the $\{Mo_2\}$ dimer, that can either be corner or edge shared, and the $\{(Mo)Mo_5\}$ pentagonal unit. This pentagonal unit is responsible for the extreme curvatures that is seen in all of these structures. These structures are so called due to their colour during synthesis/crystallisation and this is a direct result of their reduced nature. Molybdenum blues contain mixed valence Mo^{V}/Mo^{VI} metal addenda and the delocalised electrons are capable of intervalence charge transfer due to the bridging oxo-ligands which gives rise to the deep blue colour. Molybdenum browns however are much more reduced and contain direct Mo-Mo bonds, both of which are Mo^{V}, meaning the electrons are localised between these reduced centres, allowing for the characteristic brown colour.

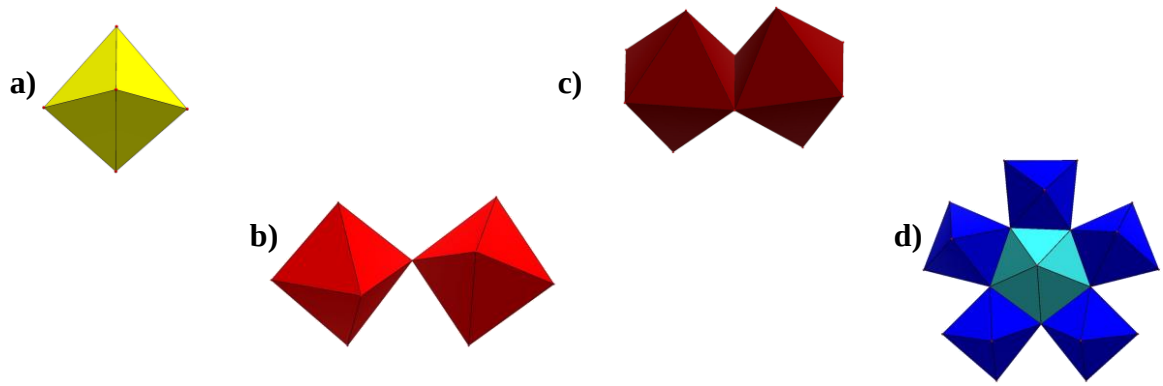

Figure 9 Polyhedral representation of the building blocks of large molybdenum clusters. a) $\{Mo_1\}$ monomer, b) corner-shared $\{Mo_2\}$ dimer, c) edge-shared $\{Mo_2\}$ dimer, d) $\{(Mo)Mo_5\}$ pentagonal unit

The synthesis of these molybdenum-based POMs is just as diverse as all POM synthesis; however, they are commonly made via simple one pot reactions and it is usually the acidification of aqueous metal salt solutions. The largest structure that can be obtained using this method is the $\{Mo_{36}\}$ type cluster and is comprised of two $\{Mo_{17}\}$ subunits linked together by two octahedral $\{Mo_1\}$ units. It isn't until a reducing agent is introduced into the system that larger structures can be made.

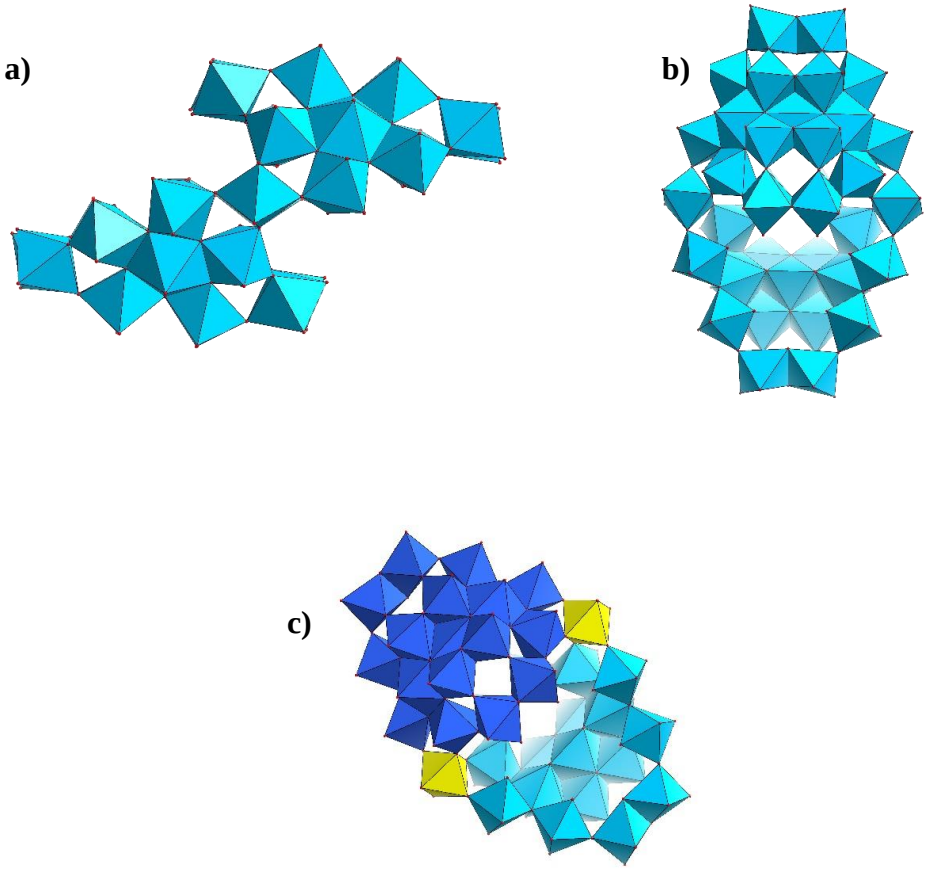

Figure 10 Polyhedral representation of {Mo_{36}} structure. a) showing side-on view, b) showing top-down view and c) highlighting the various subunits that make up the structure (the two {Mo_{17}} substructures in blue and the linking {Mo_1} subunits in yellow)

The first breakthrough regarding molybdenum blues and browns came in 1995, when Müller reported the first synthetic route and solved structure of the {Mo_{154}} giant wheel-type structure. This structure measures 4nm in diameter and has a central cavity of >2nm.[16] As well as breaking down the structure into the small building blocks previously described, the {Mo_{154}} wheel can also be thought of as a repeating {Mo_{11}} motif, which are made up of - a central {(Mo)Mo_5} pentagonal unit with two additional Mo atoms (forming an {Mo_8}), a bridging {Mo_1} unit and a linking {Mo_2} unit. Fourteen of these {Mo_{11}} subunits come together to form the {Mo_{154}}.

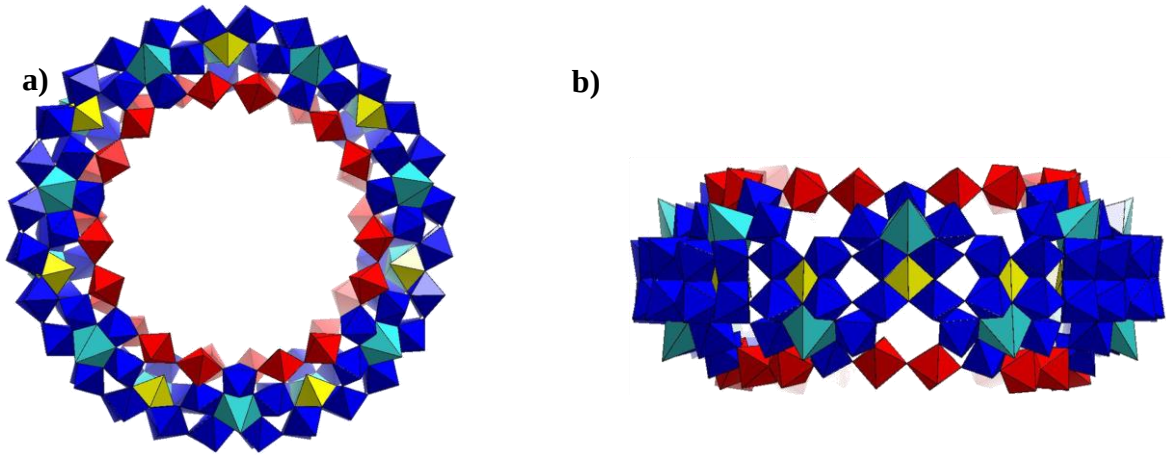

Figure 11 Polyhedral representation of the {Mo_{154}} giant wheel structure. (Colour scheme: Pentagonal {Mo_6} units = blue, dimer {Mo_2} units = red, monomer {Mo_1} units = yellow).

This discovery allowed for the continued development of the synthetic strategy regarding POMs and led to a series of wheel shaped cluster being found, such as the {Mo_{176}}[69] and the {Mo_{248}}.[70] Fascinatingly, the {Mo_{248}} is formed via a capping of the {Mo_{176}} wheel using two {Mo_{36}} cluster at each side of the wheel opening.

Molybdenum blues also encompass the largest POM known to date, also discovered by Müller. In 2002, he reported the synthesis and crystal structure of the {Mo_{368}}, otherwise known as the "blue lemon" or "hedgehog". This giant structure has 368 molybdenum metal centers, over 1000 oxygen atoms and 48 coordinated sulfate ligands. The sulfate ligands are of particular importance as they have the optimal bonding strength to be able to stabilize this giant structure and use of other acids results in smaller, more stable POMs being formed instead. It has an overall diameter of approximately 6nm and an internal cavity, that at its largest point, measure 2.5 x 4.0nm.[18]

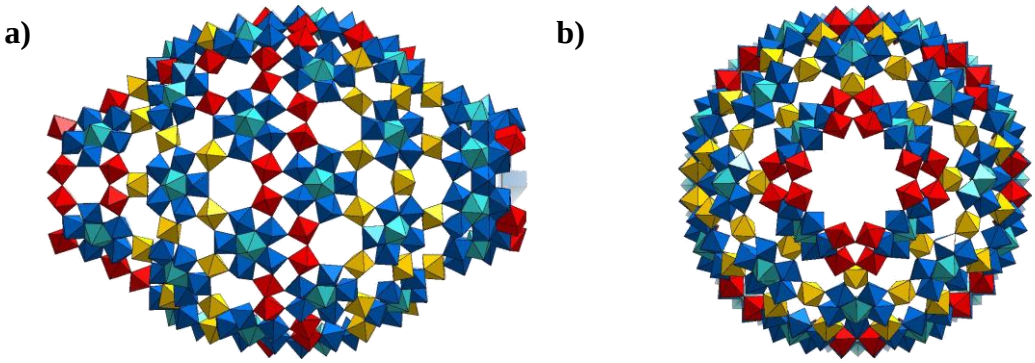

Figure 12 Polyhedral representation of the {Mo_{368}} giant "blue lemon" structure. (Colour scheme: Pentagonal {Mo6} units = blue, dimer {Mo2} units = red, monomer {Mo1} units = yellow).

However, although the structure was found almost two decades ago, only a handful of research has gone into the structure with only a few papers being published regarding the synthesis and structure. An improved synthesis was reported in 2004[71] but only characterised the structure via it's similarities in spectra such as IR and UV/Vis, both of which are highly convoluted when looking at POM structures and often don't reveal anything architecturally. A redox titration was performed to determine the number of reduced centres but again, this doesn't show that a pure product has been made. Arguably, the most important elemental analysis for POMs is X-ray crystallography, which requires high quality single crystals suitable for diffraction. Following the "improved" method doesn't provide this and so the synthesis of this POM in a high quality, single crystal yield still hasn't been achieved. This task was undertaken during this thesis as a side project and the results and features will be discussed in the results and discussion section 4.

The spherical {Mo_{132}} is the best known example of a molybdenum brown and is often dubbed the "Keplerate" structure. This was also isolated and characterized by Müller *et al.* in 1998 and consists of 132 molybdenum octahedra, with an internal spherical cavity of 1.7nm.[17] This structure can also be broken down in {Mo_{11}} units, albeit different to the ones previously described for the {Mo_{154}}. Instead, the central {(Mo)Mo_5} pentagonal unit is linked by five {Mo_2} units. These {Mo_2} units are also different as they are edge-shared rather than corner-shared, which results in the Keplerate being slightly smaller than the {Mo_{154}} with a size of 2.5nm

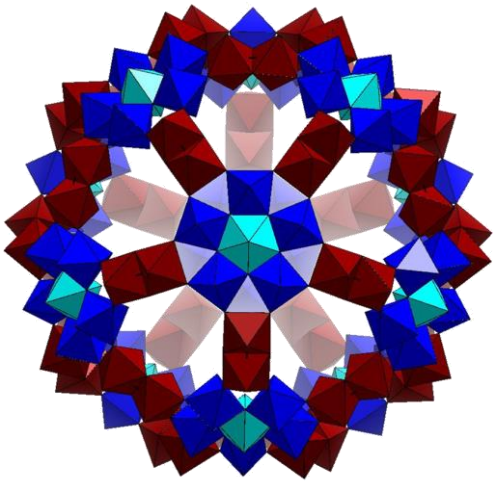

Figure 13 Polyhedral representation of the {Mo132} Keplerate structure. (Colour scheme: Pentagonal {Mo6} units = blue, edge shared dimer {Mo2} units = dark red).

which the building blocks come together to form discrete clusters is still a mystery that has evaded researchers. One of the critical reasons for this is that "in situ" analysis remains a difficult task and although studies using techniques such as NMR and IR spectroscopy have been carried out previously, they often fail to reveal anything of great value as the spectra are often extremely convoluted and difficult to interpret. Studies involving the use of mass spectrometry have revealed some important information regarding the formation of POMs. By using a combination of density functional theory (DFT) and electrospray ionization-mass spectrometry (ESI-MS), the formation mechanism for the Lindqvist POM (See 1.2.1) was proposed. This suggested that the small, symmetric cluster assembles one metal centre at a time via successive steps of protonation and water condensation reactions followed by subsequent aggregation into the final cluster.[72]

More recently, Cronin et al. utilised the use of a stopped flow system with a UV-Vis detection-based system to look at the formation of the largest molybdenum-based cluster without reducing agent, the {Mo_{36}} described previously. They found an underlying autocatalytic set whereby the {Mo_{36}} acts as a catalyst for its own formation and subsequently templates the formation of the {Mo_{154}} giant wheel structure. An expansion of this work is the basis for this thesis and more details regarding autocatalysis will be discussed later.[36]

Arguably, the lack of understanding in how these large clusters come together via self-assembly is the biggest challenge that chemists face in the design and synthesis of POMs and although the process of self-assembly tries to be directed with a specific goal in mind, it often goes a different rout due to the many factors that need to be controlled. However, this also comes with an added benefit that the discovery of new POMs is often serendipitous and the vast range of conditions that are controlled to try and direct the self-assembly allows for a wide chemical space to be explored in which novel POMs, often with interesting structural aspects, are regularly ascertained.

1.5 Introduction into autocatalysis

Autocatalysis can be briefly described as a system in which the product of a reaction acts as a catalyst for its own formation.[73] Although part of many chemical and biological systems, they were first introduced as a concept in 1890 by Ostwald for escribing chemical reactions that showed an acceleration in their rate of production as time went on. This rate increases until the reactant concentration gets too low, and a saturation has been hit and the rate of product formation plateaus. Since then, autocatalysis has been identified in a wide variety of reactions and chemical systems, ranging from simple organic reactions to complex biological networks, all of which will be discussed further. All of these reactions and chemical systems behave in a similar mechanistic way and thus, the unique kinetics of the reaction is one of the most important features of an autocatalytic system.[74]

1.5.1 General mechanism

While all systems that are autocatalytic involve the product catalyzing its own formation, there are several different chemical reaction sets by which this can occur, and each of these can be described in individual mechanistic ways, depending on how the reaction proceeds and the manner in which the autocatalyst acts. An important feature of an autocatalytic reaction is demonstrated by an initial slow positive correlation between the product concentration and time. This is followed by a sharp, exponential increase in concentration as more autocatalyst is being formed via the reaction, until the reactant concentration plateaus. This means that one of the vital signs of an autocatalytic system is a sigmoidal "S" curve when product concentration is plotted against time, although this isn't the only requirement and systems can exhibit this behavior without being autocatalytic. Even though all autocatalytic systems share similarities, each one is distinct and it's important to highlight each system and their unique elements.

1.5.2 Direct Autocatalysis

The first and simplest autocatalytic system is known as direct autocatalysis. This process can either simply be one or two reagents coming together to form a product that autocatalyses itself or involve an intermediate that catalyzes the reaction. However, although it is simple, this type of catalysis is less common, possibly due to the fact that many autocatalytic chemical systems are often complex and have a multitude of stable products that can

accelerate their own production.[75] Nevertheless, understanding the simpler mechanisms provides a good foundation for autocatalysis.

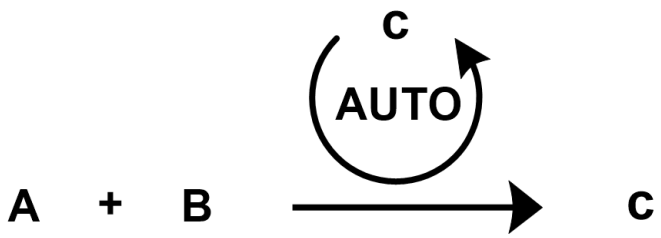

Figure 14 Scheme of autocatalysis showing how the product **C** catalyzes its own formation

One example of this type of autocatalysis is ester hydrolysis.[76] This reaction is perhaps the simplest example of an autocatalytic system and involves the reaction of an ester and water, catalyzed by acid. The reaction itself produces a carboxylic acid and an alcohol and so the acid produces can be used to catalyze its own formation.

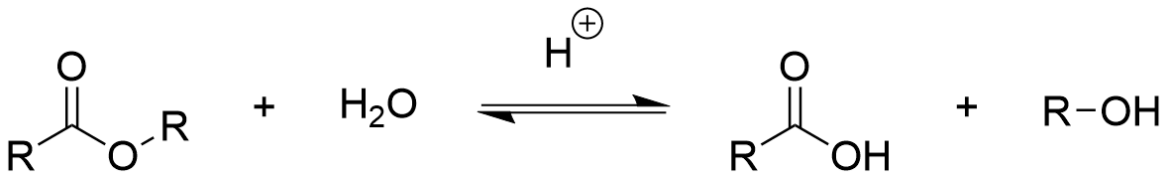

Figure 15 Reaction scheme of ester hydrolysis, showing its autocatalytic nature

1.5.4 Network Autocatalyses

Direct autocatalysis may conceptually be the simplest autocatalytic example but is not the most representative case. A similar kinetic signature can be seen in other types of autocatalysis, which falls into the realm of network autocatalysis and there are 2 different classifications within this realm. These types of autocatalysis are much more common in biological systems, as they often contain a large number of reactions within their systems which can interact in different ways. They are as follows:

1.5.4.1 Indirect Autocatalysis

The first type is known as indirect autocatalysis. This involves a system within which reagents combine to make a product, but the reactant and products never directly interact with each other. One example of this is the biological system of glycolysis.[77] In this example, glucose is broken down into pyruvate with the addition of adenosine triphosphate (ATP) being generated. This autocatalytic nature comes into effect as this multistep system has to use ATP in order to start the first reaction of glucose into glucose-6-phosphate. Without this positive feedback loop involving ATP as an autocatalyst of its own production, the system would collapse.

1.5.4.2 Collective Autocatalysis

The second system that falls under the network autocatalysis bracket is *Collective Autocatalysis*. This involves a process in which no product influences its own formation but that of other reactions in the system in a way that means the whole set of products catalyze their own formation within a self-sustaining and closed system.[78] This type of autocatalysis is often thought to have played a role within the origin of life as sets of chemical reaction would have grown and evolved into larger and more intricate networks leading up to the complex yet spontaneous formation of RNA.

Autocatalysis is a fundamental process in chemistry and has given rise to a multitude of different reactions, products and processes. From replication of simple organic molecules to possibly playing a role within the origin of life, it is embedded within the foundations of chemistry. As well as chemistry, autocatalysis can be extended into society, economics and even technological advancement in such a way that it has a substantial effect in everything we do.[79]

1.6 Monitoring Autocatalysis

One of the signatures of an autocatalytic reaction lies in the kinetics of the reaction. Autocatalytic reactions uniquely exhibit a sigmoidal shaped curve when product concentration is plotted over time. This sigmoidal curve can be broken down into three phases: (i) the induction period, (ii) the exponential phase and (iii) the saturation phase, each of which can be easily explained. The induction/lag period occurs due to there being no autocatalyst yet formed and so the transformation of reactants into products is very slow and

occurs via an uncatalyzed pathway. However, once the autocatalyst is reaches a critical concentration it facilitates an exponential increase for itself. Later, as the reactants are used up, the rate of product formation begins to decay, and thus a saturation phase is seen.

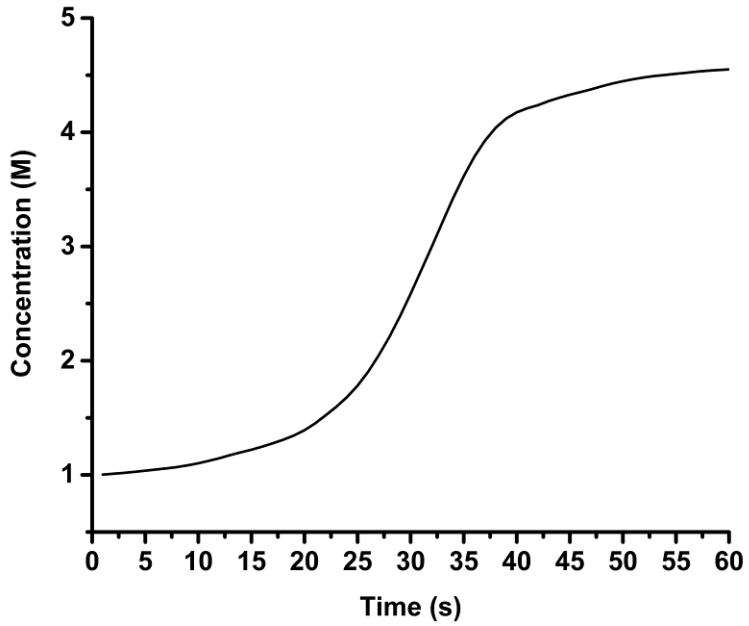

Figure 16 General sigmoidal curve. Each distinct part can be seen as a lag period in the beginning, followed by exponential increase and finally kinetic saturation

Although many different forms of autocatalysis can occur in many different reactions as outlined in the previous chapter, an analysis of the kinetic rate equation of the simplest autocatalytic systems proves useful in order to understand the behavior of these systems. The kinetic rate equations for the simplest autocatalytic system, direct autocatalysis, will be the only type of system looked at as the other systems become much more complicated as a multitude of products and reactants can be involved and the number of rate constants involved would become extremely convoluted. However, the rate equations for direct autocatalysis form a good basis for the overall understanding of how all autocatalytic systems behave.

As stated previously, an autocatalytic reaction is so if at least one of the products acts as a catalyst in the formation of itself. This results in an interesting property that the rate equations are nonlinear i.e., the reaction is slow in the beginning but increases as the reaction proceeds and more product is formed, until a plateau is reached. The simplest possible autocatalytic reaction is as follows:

$$A + B \rightarrow 2B \tag{1}$$

Then, using the law of mass action, the forward reaction is the rate of change of reactant concentration and is equal to $k_1[A][B]$ and the reverse reaction is the rate of change in the product formation and is equal to $k_2[B]^2$. This can be made into equation (2) as follows:

$$\frac{d[B]}{dt} = -\frac{d[A]}{dt} = k_1[A][B] - k_2[B]^2 \tag{2}$$

Where k_1 and k_2 are the rate constants and [A] and [B] are the reactant and product concentrations. Assuming that the rate of the forward reaction is much faster than the rate of the reverse reaction i.e., $k_1 >> k_2$, the rate equation can simplify to equation (3) as follows:

$$-\frac{d[A]}{dt} = k_1[A][B] \tag{3}$$

If it is assumed that $[A]_0$ is the concentration of reactant A at the start of the reaction and $[B]_0$ is the concentration of the catalyst at the start of the reaction, then $[A]_0 - [A] = [B] - [B]_0$ and equation (3) can be directly solved. This yields reaction (4) as follows:

$$-\frac{d[A]}{dt} = k_1([A][A]_0 + [A]_0[B]_0 - [A]^2 \quad (4)$$

Rearranging the equation and integrating yields equation (5):

$$-\int k\,dt = \int \frac{1}{[A][A]_0 + [A]_0[B]_0 - [A]^2} d[A] \quad (4)$$

Integration of this equation obtains the following solutions:

$$[A] = \frac{[A]_0 + [B]_0}{1 + \frac{[B]_0}{[A]_0} \cdot e^{([A]_0 + [B]_0)kt}} \quad (5)$$

And

$$[B] = \frac{[A]_0 + [B]_0}{1 + \frac{[A]_0}{[B]_0} \cdot e^{-([A]_0 + [B]_0)kt}} \quad (6)$$

These equations describe a logistic equation and are responsible for the sigmoidal curve seen when reactant or product concentration is followed.

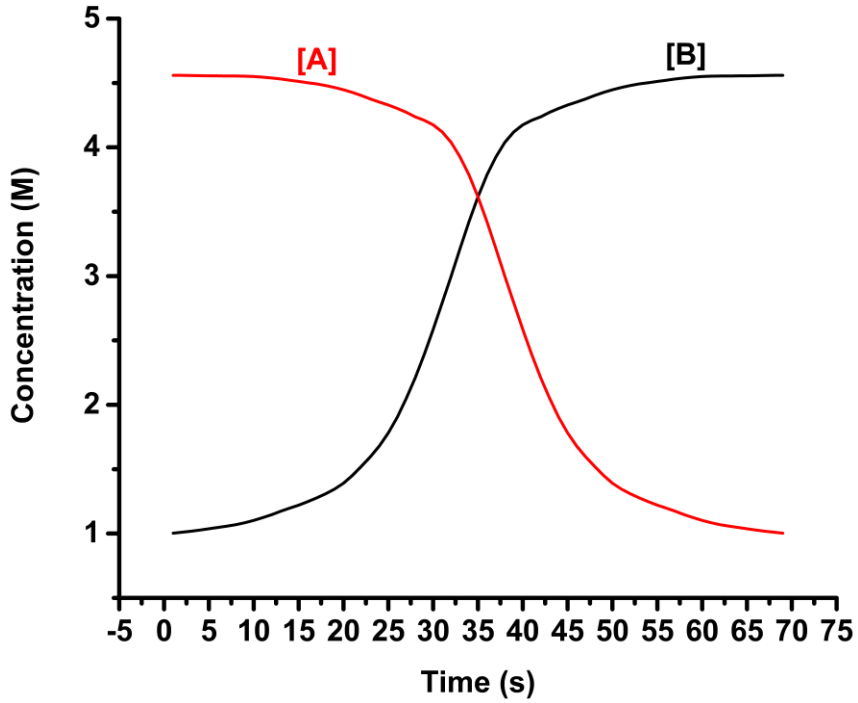

Figure 17 Sigmoidal curves when equations (5) and (6) are plotted showing reactant and product concentration over time

1.7 Examples of autocatalytic sets

As described above, autocatalytic reactions can have various different pathways and mechanisms which translates to a diverse set of reactions. In order to better understand autocatalysis, it is helpful to view real world examples, from simple chemical reactions to biological systems:

1.7.1 Organic reactions – Chemical Clocks:

Starting with a relatively simple reaction, one of the most well-known examples of autocatalytic sets are known as chemical clocks. The kinetics and nature of these systems has been studied extensively and can even be manipulated in such a way that the lag time of the sigmoidal nature can be, in a sense, programmed. One specific case of chemical clocks and their behavior involves the use of the hydrolysis of cyclic esters and their effect on the bromate-sulfite (BS) reaction.[80]

(7)

(8)

In the first step of the BS reaction, sulfite reacts with a single hydrogen ion to produce hydrogen sulfite, which can be seen in equation (7). This hydrogen sulfite is then involved in a second reaction with bromate to produce bromide, sulfate and 3 hydrogen ions, as can be seen in equation (8). These 3 hydrogen ions can then be used for equation (7), causing an exponential decrease in the pH as more acid is produced. However, for this system to work, there must be an initial source of protons in the system, which is where the programmable nature of this reaction can be seen. As described in a previous chapter, the hydrolysis of esters produces acid, which is used in its autocatalysis. Following on from this, depending on the ester that is used and its concentration, the time of hydrolysis varies and can be manipulated in a way that allows the lag time of the BS reaction to be accurately manipulated, as a slower release of protons into the system will extend the lag period.

1.7.2 Formose Reaction

Moving on to a more complex example and one that is biological in nature - the Formose reaction was first noted by Butlerov in 1861 and a mechanism was later proposed by Breslow in 1959. In the Formose reaction, formaldehyde is involved as the feedstock for an autocatalytic cycle that produces a number of different sugars, most notably ribose, meaning that this reaction could have played an important role in the emergence of RNA.[81]

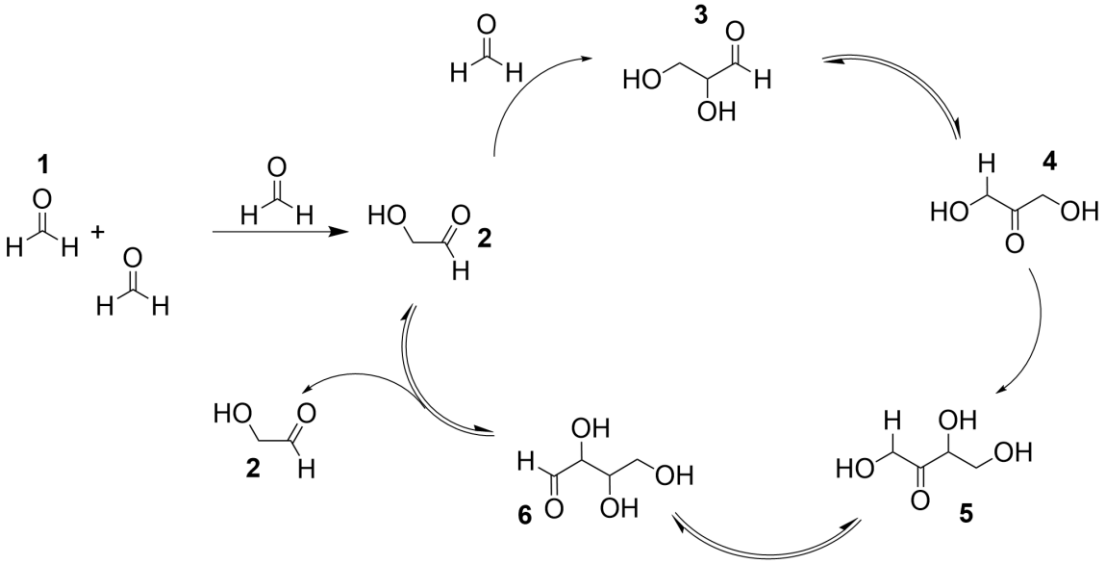

The reaction starts by the combination of two formaldehyde molecules **(1)** combining to make glycolaldehyde, which is a kinetically slow reaction and is the cause of the lag period seen in this reaction. This can be seen in the initial step outside of the cycle in reaction (10). However, once this step has been completed, glycolaldehyde **(2)** reacts readily with formaldehyde **(1)** in an aldol condensation to produce glyceraldehyde **(3)**. The glyceraldehyde can then tautomerize into dihydroxyacetone (DHA) **(4)**, which reacts with another glyceraldehyde to produce tetrulose **(5)**, which can go on to form a number of different pentose sugars. Alternatively, and the route of autocatalysis, tetrulose can undergo ketose-aldose isomerization and form aldotetrose, which can undergo a retro-aldol reaction to yield 2 molecules of glycolaldehyde. This net production of 2 molecules of glycolaldehyde from a single molecule is where the autocatalytic nature of this reaction can be seen.[82] During the cycle DHA can also react with glycolaldehyde, which forms ribulose and this can isomerize into ribose, which is an important building block of ribonucleic acid, highlighting the importance of such autocatalytic systems in biology. The formation of a complex sugar such as ribose from a simple formaldehyde molecule could be one of the complex mechanisms that occurred during the origin of life that allowed the production of RNA, highlighting how important an autocatalytic cycle could be.

1.7.3 DNA Replication

Finally, the last and arguably most important occurrence of an autocatalytic system is the replication of DNA. Although relatively simple in its mechanism i.e., DNA replication occurs via a strand of DNA templating the production of more strands of DNA thus allowing for an exponential increase, its importance cannot be understated. An example of direct autocatalysis, thanks to the selective association of complementary nucleotide bases and so one strand can only be involved in one templation. Although the initial appearance of DNA is still unclear, and there are many theories as to the emergence of RNA, autocatalysis being at the center of its replication system highlights the importance of autocatalytic sets.

Autocatalytic sets can range from simple organic reactions to complex biological systems and all the way up to life itself. The importance of autocatalysis has been highlighted throughout and will continue to be of relevance and importance for the future. However, biological systems and the replication of DNA may be well understood but their emergence is still a mystery that remains. Extending autocatalytic sets to well-known building blocks of inorganic materials may provide an insight into how these systems came to fruition.

1.7.4 MOFs/POMs:

A small number of autocatalytic examples can be seen in structures known as metal organic frameworks (MOFs). These are organic-inorganic hybrid structures that consist of metal ions surrounded by organic linker molecules, which are then bonded together to form repeating cage like structures. They are highly diverse in structure, with tunable porosity, flexibility, topology, and functionality. Owing to this, they have a wide range of applications, including catalysis, energy storage and liquid or gas separation.[83]

One example of autocatalysis in MOFs is not an application of MOFs itself but instead it is the formation of a MOF that is autocatalytic. UiO-66 is made up of $[Zr_6O_4(OH)_4]$ clusters with 1,4-benzodicarboxylic acid linkers and is highly stable. During the formation of this MOF, $ZrCl_4$ undergoes hydrolysis into zirconyl chloride species, which is followed by the arrangement of these clusters into the hexanuclear building blocks via an acid catalyzed process that then crystallizes into UiO-66. The exact pathway is unknown; however, it is certain that this crystallization is facilitated by the loss of protons. As the

process of the clusters into building blocks is acid catalyzed, this is where the autocatalytic nature of its nucleation can be seen. Furthermore, the transformation of multinuclear species into the hexanuclear building blocks cannot proceed without acidic conditions, so it would be possible to control the nucleation in a similar way to chemical clocks.[84]

Polyoxometalates (POMs) are a different class of inorganic molecules that can be described high oxidation metal oxide clusters. They are known to have a variety of chemical and physical properties but perhaps the most intriguing thing is their formation. Although it is widely accepted that POMs are made up of smaller building blocks and these come together to make larger and more complex structures via a self-assembly and templation process, the exact way in this occurs is still not fully understood. One subset of POMs is known as molybdenum blues and are high nuclearity clusters consisting of reduced molybdenum atoms linked by oxygen that often show high complexity in structure and can also incorporate a wide range of heteroatoms. Examples include Mo_{36}, Mo_{154} and Mo_{368}, which is the largest POM recorded to date.

During the synthesis of molybdenum blues, a multitude of stable products are formed before a reducing agent is added, including the Mo_1 monomer, Mo_2 dimers, the Mo_6 and the Mo_{36} subunits, which is the largest possible structure in the absence of a reducing agent. Although the self-assembly process is not fully understood, the formation of Mo_{36} has recently been shown to be autocatalytic. The process can be seen during the synthesis of the larger Mo_{154} molybdenum blue, as this is templated by the Mo_{36} cluster. The kinetics was investigated using a stopped-flow system to monitor the formation of the Mo_{36} and a sigmoidal evolution was seen. The addition of preformed Mo_{36} during the synthesis eliminated any lag period, a further indication of an autocatalytic system. It is thought that the Mo_{36} acts as a template and promotes the formation of Mo_6 subunits, which in turn are used in the synthesis of the Mo_{36} itself, thus catalyzing its own formation. This autocatalytic set is of large importance as it shows that information rich systems are capable of self-replication out outside of biology and also helps the understanding of POM self-assembly as a whole.[36]

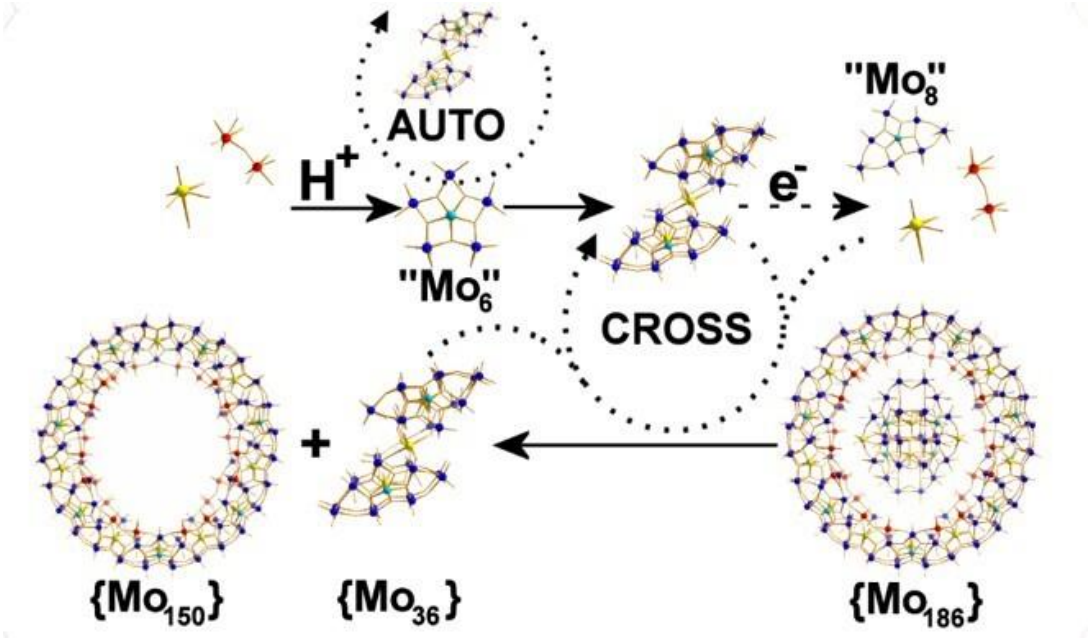

Figure 18 Autocatalytic and cross-catalytic cycles in the synthesis of {Mo154-x} wheels. Taken from reference 36 with permission

Understanding the underlying mechanisms that govern the self-assembly of POMs could be the key step in unlocking access to larger structures beyond the Mo_{368} and could be vital in improving synthetic yields and the possibility of designing new materials involving the use of POMs.

Autocatalysis has been shown to be important in organic, inorganic, and biological systems and plays a vital role in chemistry. From simple reactions to the origin of life, autocatalysis can provide an explanation for the kinetics and mechanistic features of a wide range of reactions.

2 Aims and Abstract

The term self-assembly is used as a 'catch-all' term to describe the formation of many molecules and supramolecular architectures but often the precise mechanism of assembly is neglected. In the following pages, we have investigated the kinetics of the self-assembly of one of the simplest heteropolyoxoanion, the Keggin ion $[XMo_{12}O_{40}]^{x-}$.

In tackling this problem, we were seeking to observe the very fast kinetics that were happening at the start of the reaction. Previous work had established an autocatalytic system and knowing if this happens for all Keggin clusters would be a huge insight into the formation of POMs. The use of a UV/Vis detection-based system will be used, with the capacity to slow the reaction down to 5°C to catch the kinetics at the start.

Finally, we will seek to explore the effect of the heteroatom on the kinetics of the autocatalytic process by investigating and comparing the rates of formation of $\{AsMo_{12}\}$ and $\{SiMo_{12}\}$, which would allow further insight into how the heteroatom template affects the formation of the cluster.

Additionally, if the experimental data provides evidence of an autocatalytic formation pathway for the POMs under investigation, a computational stochastic model will be implemented in order to probe the reason why such a well-defined library of gigantic Mo-based nanostructures exists and the role of the generations of the autocatalytic sets which perhaps construct a network that operates at criticality. This would allow the building blocks to be incorporated into precisely defined cluster nanostructures, rather than give a combinatorial explosion of products.

Understanding the process of self-assembly, even in small, simple structures like the Keggin is an important start into understanding how simple metal salts come together to form information rich clusters with distinct architectures and could allow an opportunity for larger or more complex new structures to be discovered.

3 Investigation of Autocatalysis in Keggin-based POM Clusters

3.1 Introduction into Autocatalysis and Previous Experiments

The term self-assembly is used as a 'catch-all' term to describe the formation of many molecules and supramolecular architectures but the precise mechanism of assembly is often neglected. Here we have investigated the kinetics of the self-assembly of one of the simplest heteropolyoxoanions, the Keggin ion $[XMo_{12}O_{40}]^{x-}$. This study shows that the Keggin ion is able to catalyze its own formation via an autocatalytic cycle, seen when using variable temperature UV/vis spectroscopy. Kinetic investigations with real-time monitoring of the formation reaction of the $[XMo_{12}O_{40}]^{x-}$ family revealed key traits of autocatalytic systems including kinetic saturation, and these were explored using a stochastic model which confirms our experimental observations. Finally, we explore the effect of the heteroatom on the kinetics of the autocatalytic process by investigating and comparing the rates of formation of $[AsMo_{12}]$ and $[SiMo_{12}]$.

Polyoxometalates (POMs) have been widely studied, largely due to the fact they cover a vast range of shapes, sizes, and properties.[85–89] One of the fundamental aspects of POMs is their ability to self-assemble to discrete molecular structures, despite the presence of building block libraries that could combinatorically form an infinite number of alternative structures. These discrete structures range from small clusters such as the $\{Mo_8\}$ (0.7 nm), the $\{Mo_{12}\}$ Keggin (1.0 nm) and the $\{Mo_{36}\}$ (2.1 nm), all the way up to the high nuclearity nanosized species of $\{Mo_{132}\}$ Keplerate (2.9 nm), $\{Mo_{154}\}$ (3.6 nm) Molybdenum blue wheel and the protein sized, and largest of all POMs, $\{Mo_{368}\}$ (5.5 nm). Although the process of self-assembly still isn't fully understood, recent studies have shown that both the $\{Mo_{36}\}$ and the $\{PMo_{12}\}$ Keggin are involved in the assembly of larger POM structures via a template mediated process as part of a set of autocatalytic reactions, but it is not known how the smaller clusters form. This is important since the Keggin species is the oldest known POM archetype which was first discovered in 1826.[90] However, it wasn't until over a century later that its structure was determined by X-ray crystallography in 1933[91] and it's now, after almost another century has passed, that the intrinsic formation mechanism is being investigated. The lack of earlier mechanistic insights did not prevent the investigation of its chemical reactivity along with other heteropolyanions which are by far the most explored

subset of the POM family.[92–96] These can be described as metal oxide clusters that incorporate heteroatoms such as PO_4^{3-} and SO_4^{2-}.[97]

Investigations into the self-assembly and dynamics of these POM systems has often involved the use of high-resolution mass spectrometry, specifically electrospray (ESI-MS) and cryospray (CSI-MS), as these ionization techniques are mild enough to prevent undesirable fragmentations and allow well-defined identification of structurally related species within the reaction systems. These studies, along with theoretical studies, have allowed us to gain insight into how these complex systems fundamentally behave and how the identified clusters isomerize, speciate and reassemble.[98–105] Decades of extensive investigations on POM's accompanied by detailed structural characterizations has allowed the discovery of numerous species. The breakdown into various subgroups such as iso-/hetero-polyanions, molybdenum blues/browns and identification of fundamental virtual building blocks, has been essential for the deeper understanding POM's chemical reactivity.

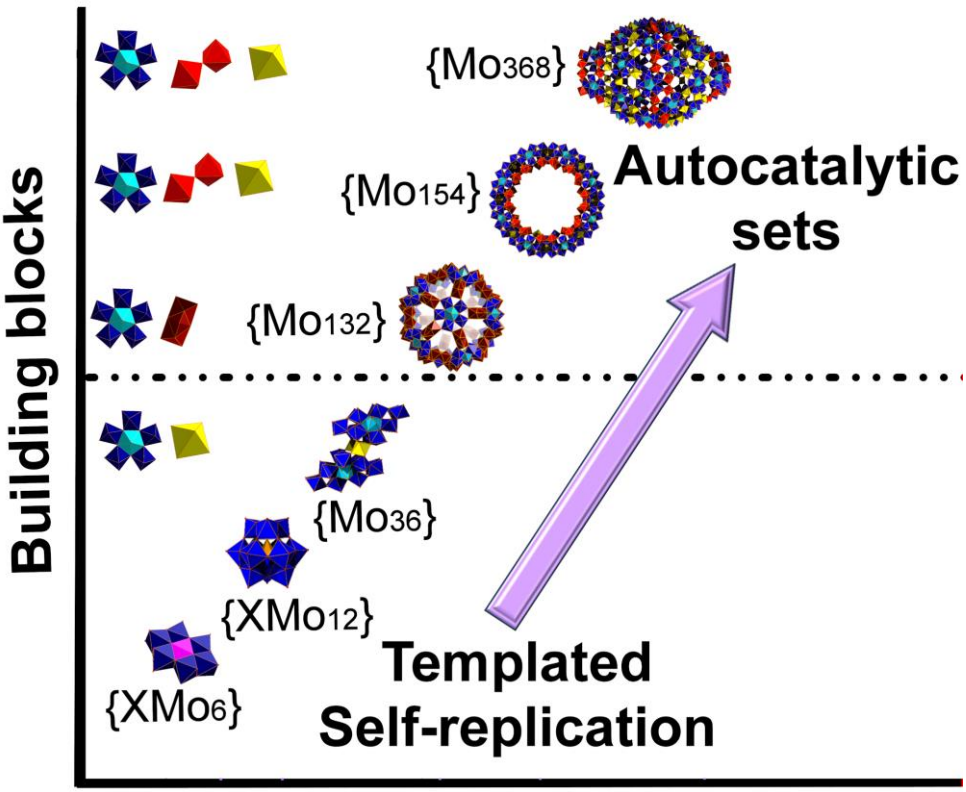

Figure 19 Breakdown of molybdenum POM classification. Virtual building blocks (VBB) have not been isolated but are known to be building blocks for high-nuclearity POMs. Isopolyanions (Iso) and heteropolyanions (Het) are isolated and stable clusters.

However, although extensive studies have probed the self-assembly at the conceptual level or theoretical studies probing the bonding,[106–109] it has been difficult to devise a mechanistic and experimental paradigm to investigate the mechanism of the formation. Previously it has been shown that the large polyoxometalates just as the {Mo_{154}} wheel and {Mo_{132}} ball shaped clusters are formed by a network[110] of mutually catalytic reactions – a so called autocatalytic set – and this explains why these clusters are even possible and represent magic numbers of stable compounds from the infinite number conceivable. This is important since it hints at the first example of the transfer of templated-based information at the molecular level in an inorganic system outside of biological ones.[111,112]

Autocatalytic processes are reactions in which a product of the reaction acts as a catalyst for its own formation. One of the characteristic traits of autocatalytic systems[113–116] is the existence of an induction period, followed by an exponential rise in rate. Finally, the system reaches a plateau in product concentration as the reactants are used up, and overall the plot of concentration vs time is sigmoidal relationship.[117] Additionally, self-replication phenomena might take place at the same time, in the case where the product or species of the autocatalytic set, template their own formation which results ultimately in the amplification of the reaction rate. More specifically, a marked increase of the reaction rate takes place as a function of time followed by a considerable decrease upon formation of substantial amount of product. The use of the term is appropriate only for chemical systems considered under constant temperature and pressure. Crucially, the identification of autocatalytic and self-replication effects does not depend only on the detection of an induction period but rather on a collection of signatures associated with this process, such as exponential (sigmoidal) product vs. time curve with induction period, rate increase and elimination of induction period upon seeding of the reaction mixture with pre-formed product followed by kinetic saturation of the system and deceleration of the species' formation. In this work we hypothesized that the template-mediated autocatalysis of POMs provides crucial information in relation to the driving force that directs the assembly of these chemical systems. That is, the formation of discrete products out of a plethora of infinite combinations is only possible due to the selective utilization of building blocks that can be recognized and take part in the autocatalytic cycle, such as {Mo_1}, {Mo_2}, {Mo_3}, {XMo_3} and {Mo_6}, as these are able to carry specific chemical and structural information. Given the importance of lower nuclearity species, due to their involvement in larger autocatalytic sets and cross-catalyzed systems that produce nanosized high nuclearity molecular metal oxides, we envisaged to investigate and identify the autocatalytic behavior of different species that

belong to the Keggin family of molecular metal oxides with the general formula $[XMo_{12}O_{40}]^{x-}$ (X = P, As or Si) – $[AsMo_{12}O_{40}]^{3-}$ and $[SiMo_{12}O_{40}]^{4-}$.

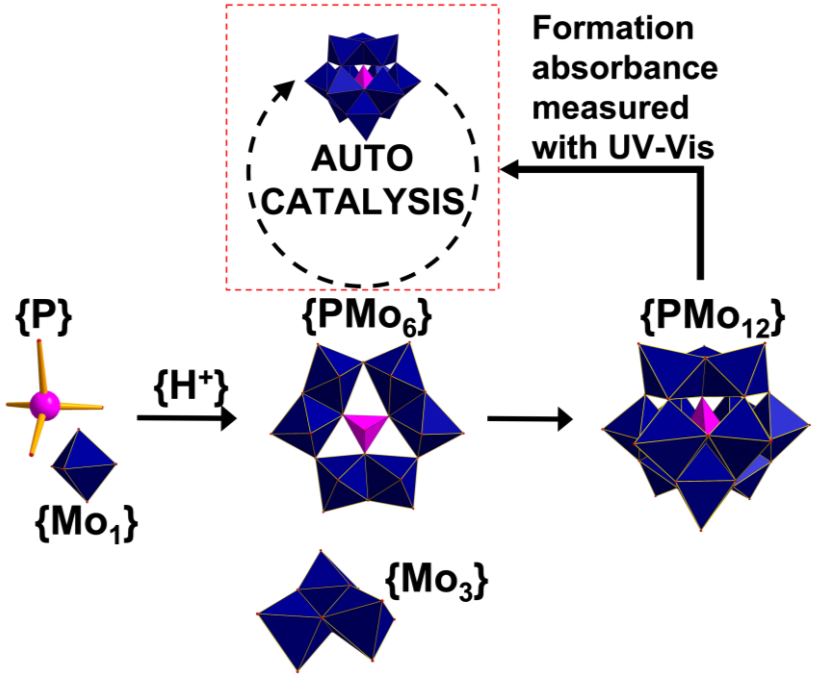

Figure 20 Formation of $\{PMo_{12}\}$ Keggin species via a $\{PMo6\}/\{Mo_3\}$ templated autocatalytic cycle. Formation of $\{PMo_{12}\}$ was previously monitored using stopped flow UV-Vis to probe autocatalytic nature via a sigmoidal increase in absorbance.

Preliminary results indicated previously that the formation of the $\{PMo_{12}\}$ anion follows an autocatalytic pathway and very fast kinetics. The use of a stopped-flow UV-vis apparatus was necessary in this case to monitor the reaction kinetics which was carried out by mixing freshly prepared solutions of $Na_2MoO_4 \cdot 2H_2O$, and H_3PO_4 / $HClO_4$ allowing us to identify the characteristic signature of autocatalytic systems. This provided the first hint that autocatalysis may be common and not an artefact among the members of the Keggin family. The obtained information offers a unique opportunity for the exploration of the other members of the Keggin family and allow us to determine if the autocatalytic traits and the fast kinetics of the $\{PMo_{12}\}$ Keggin are inherent properties of the whole Keggin family. Thus, this offered the opportunity to widen the search to other heteroatom templated Keggins and the possibility of seeing further evidence of their autocatalytic nature. The novel experiments for this thesis carried out were focused on the formation of $\{AsMo_{12}\}$ and $\{SiMo_{12}\}$ and are detailed in the next section.

3.2 Novel Experiments and Data

3.2.1 Initial Reaction

Continuing on from the previous experiments that already determined an autocatalytic formation pathway for {PMo_{12}}, here we will discuss our experimental efforts to monitor the formation mechanism of the {$AsMo_{12}$} and {$SiMo_{12}$} species where the use of a conventional UV/Vis detection system, equipped with a temperature control, proved to be sufficient. The first set of data obtained is for a reduced version of the $[AsMo_{12}O_{40}]^{3-}$ Keggin, where freshly prepared solutions of $Na_2MoO_4{\cdot}2H_2O$, ascorbic acid and $Na_2HAO_4{\cdot}7H_2O$ were mixed inside a 10 mm cuvette at quantities of 0.5, 0.5 and 2 mL respectively. The reaction was carried out at 5°C as we recorded the real time λ_{max} of the UV-vis signal centered at 800 nm (Figure 20). Interestingly the increase of the concentration of the species formed in solution as a function of the time followed a sigmoidal trend, which is indicative of an underlying autocatalytic process.

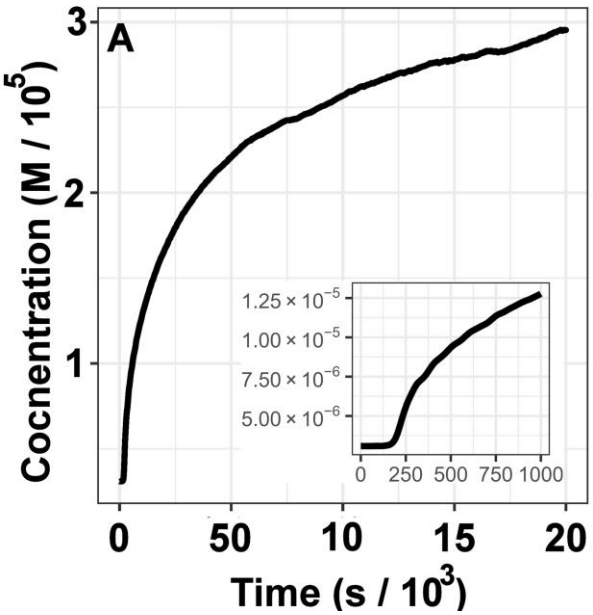

Figure 21 Concentration vs. time profile of {$AsMo_{12}$} (in H2O at 5°C), initial concentrations [Mo] = 0.02 M, [H+] = 0.028 M, [As] = $5x10^{-3}$ M. Inset of graph showing lag period at the start of the reaction.

In an effort to further investigate the potential effect of the heteroatom on the catalytic cycle and to determine if the autocatalysis is a general property of the Keggin family and not heteroatom specific, we investigated the formation reaction of the reduced {$SiMo_{12}$} Keggin in a similar manner. The same UV/Vis set up was used, under the same experimental

conditions. This time freshly prepared solutions of $Na_2MoO_4 \cdot 2H_2O$, ascorbic acid and Na_2SiO_3 were used. Although this reaction was carried out at twice the concentration, the reaction is much slower when compared to the formation of {$AsMo_{12}$} Keggin species. The characteristic incubation period was detected in a similar fashion, providing evidence that the formation reaction of this system also proceeds via an autocatalytic cycle (Figure 21).

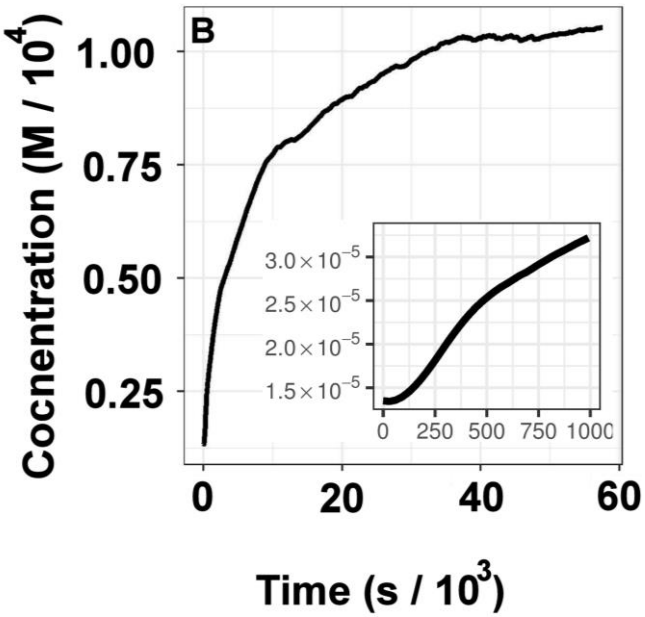

Figure 22 Concentration vs. time profile of {$SiMo_{12}$} (in H2O at 5 °C), initial concentrations [Mo] = 0.02M, [H+] = 0.028M, [Si] = 5x10-3M. Inset of graphs shows lag period at the start.

3.2.2 Temperature Variation Experiments for $AsMo_{12}$

Subsequently, to further verify the kinetic behavior of the underlying autocatalytic cycle, we carried out the same reactions using the same stock solutions at various increasing temperatures, as this would result in an increase in the rate of the reaction and therefore an increase in the concentration of the species produced as a function of the time. It would also help to provide further evidence and verify that the presence of the incubation period is not an experimental artefact of the UV-vis system. Indeed, the temperature increase of the reaction mixture gradually eliminated the lag period that had been observed in the system due to the increased production rate of {$AsMo_{12}$} species, further supporting the hypothesis of an autocatalytic system (figure 22A and 22B).

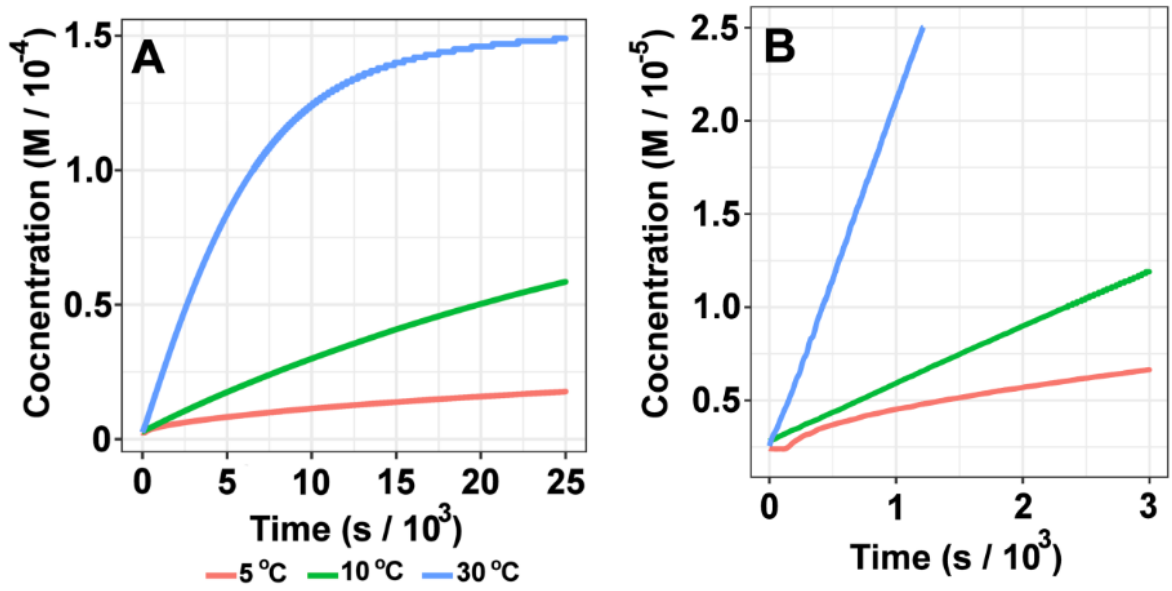

Figure 23 (A) Concentration vs. time profile of {$AsMo_{12}$} H2O, initial concentrations [Mo] = 0.01 M, [H+] = 0.014M. The data represents the concentration profile vs. time of the same reaction at various different temperatures **(B)** Inset of Graph (A), showing disappearance of lag period upon increased temperature

3.2.3 Seeding Experiments for $AsMo_{12}$

Since the presence of the incubation period is not a sufficient enough requirement on its own to verify the presence of autocatalysis, it was envisaged that the autocatalysis occurs via a molecular recognition process where the presence of a species is required in order to act as a template for the further formation of another cluster in the reaction mixture. A key feature of autocatalytic systems is that during the initial stages of the reaction, the process occurs primarily via an uncatalyzed pathway which is the cause of the observed lag time. However, once a minimum concentration of the catalyst is formed in solution, initiate the autocatalytic cycle. Therefore, introduction of pre-synthesized {$AsMo_{12}$}, at the beginning of the reaction, (t = 0), should result in the elimination of the induction period in the rate profile for the reaction, and an increase of the initial rate. In order to verify our hypothesis, an amount of the preformed {$AsMo_{12}$} (0.05 mL) was added at incrementally increasing concentrations into the original mixture and the reaction was followed with UV-vis spectroscopy once more as a function of the time at 800nm. This pre-synthesized {$AsMo_{12}$} was made up to 6 different solution concentrations – 1.19 x 10^{-7}, 3.83 x 10^{-7}, 5.73 x 10^{-7}, 7.65 x 10^{-7}, 1.16 x 10^{-6} and 1.53 x 10^{-6} M.

.

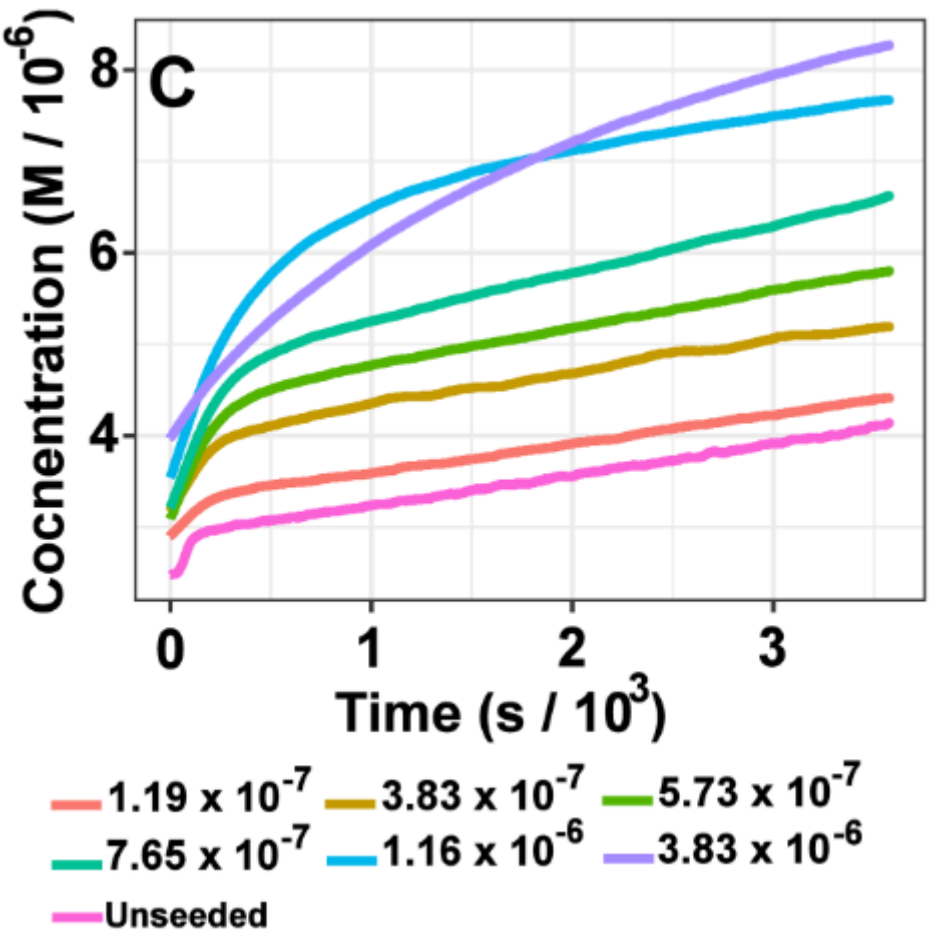

Figure 24 Concentration vs. time profile of {$AsMo_{12}$} (in H2O at 5 °C), initial concentrations [Mo] = 4 x 10–3 M, [H+] = 5.65 x 10–3 M. The data represents the concentration profile vs. time of the same reaction mixture seeded with preformed {$AsMo_{12}$}

The most prolific change when there is addition of a seed is the gradual elimination of the lag period (Figure 23), providing further support and reinforcing the hypothesis that the {$AsMo_{12}$} is formed via a template mediated process whereby the cluster autocatalyses its own formation. As shown in Figure 24, auto-catalyst saturation occurs after addition of $1.16x10^{-6}$ M of preformed {$AsMo_{12}$}, inducing maximization of the self-propagated rate of {$AsMo_{12}$}, as expected.

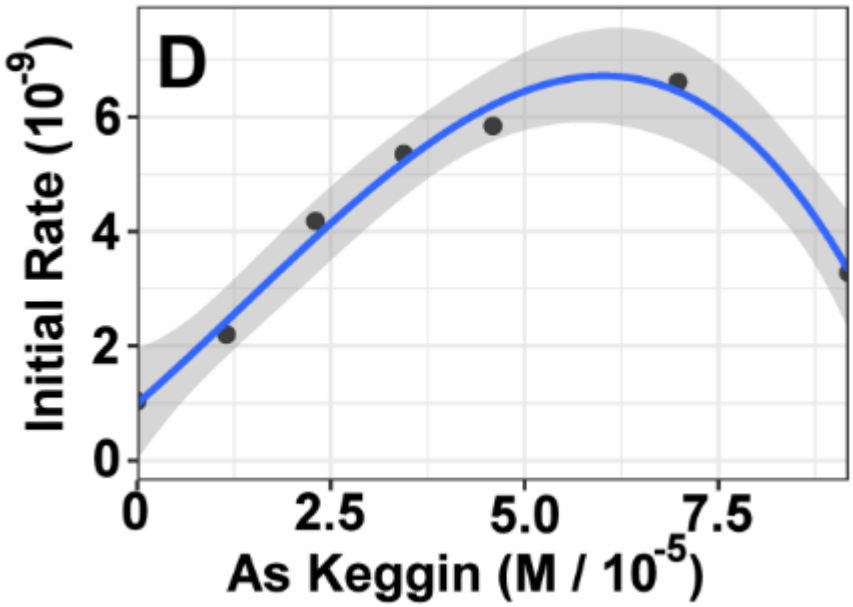

Figure 25 Kinetic saturation of {$AsMo_{12}$} autocatalyst. Formation rate vs. concentration of {$AsMo_{12}$} (Cx10-5 M) injected in the reaction mixture (in H_2O at 5 °C). The experimental data points represent the initial rate of the system. An increase is observed at the beginning before reaching a plateau (saturation).

3.2.4 Temperature Variation Experiments for $SiMo_{12}$

These results encouraged us to further investigate the behavior of the {$SiMo_{12}$} system at various temperatures, in a similar way to described previously for the {$AsMo_{12}$}, and more specifically on the incubation period. Indeed, the temperature increase also led to the gradual elimination of the incubation period due to the increased production rate of the {$SiMo_{12}$} Keggin species (Figure 25).

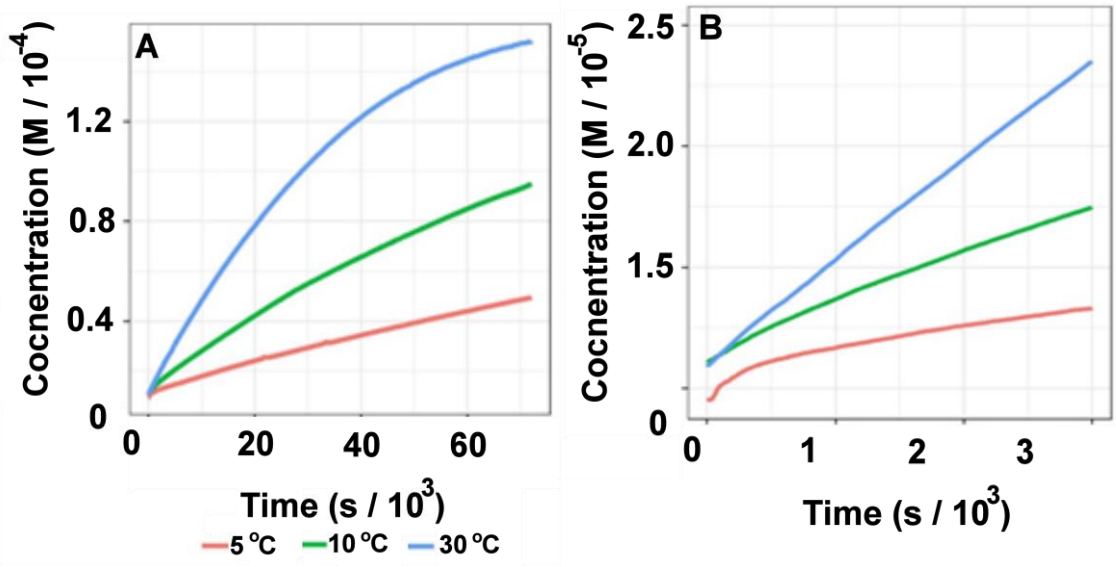

Figure 26 Concentration vs. time profile of {$SiMo_{12}$} in H_2O, initial concentrations [Mo] = 0.01M, [H^+] = 0.014M. The data represents the concentration profile vs. time of the same reaction at various different temperatures **(B)** Inset of Graph (A), showing disappearance of lag period upon increased temperature.

3.2.5 Seeding Experiments for $SiMo_{12}$

Finally, the additional verification of the presence of autocatalytic cycle in the system involved the seeding of the reaction mixture with preformed {$SiMo_{12}$}, much like the {$AsMo_{12}$}, but at an increased concentration and volume. This pre-synthesized {$SiMo_{12}$} was made up to 5 different solution concentrations: 4.78×10^{-7}, 9.12×10^{-7}, 1.92×10^{-6}, 2.87×10^{-6} and 3.83×10^{-6} M.

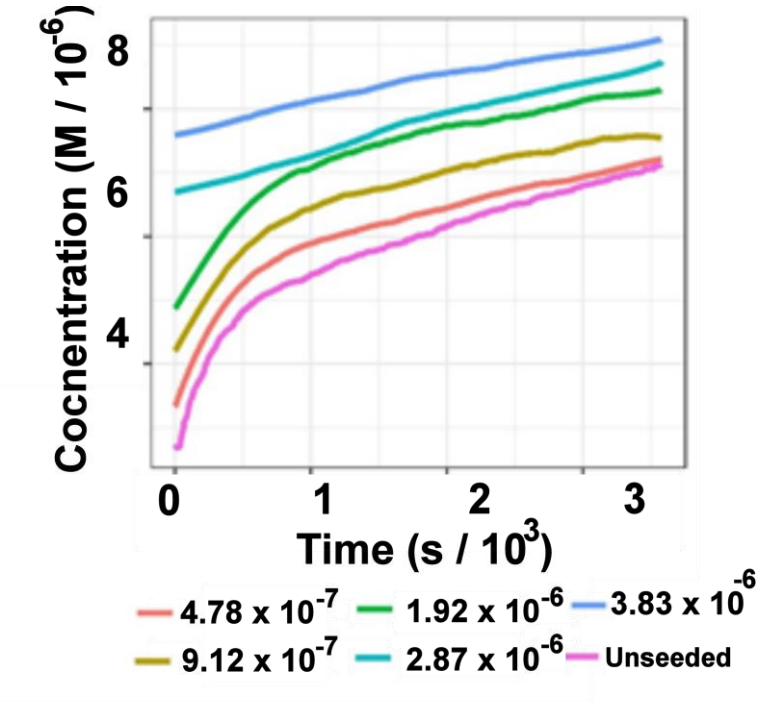

Figure 27 Concentration vs. time profile of {$SiMo_{12}$} (in H2O at 5 °C), initial concentrations [Mo] = 4 x 10–3 M, [H+] = 5.65 x 10–3 M. The data represents the concentration profile vs. time of the same reaction mixture seeded with preformed {$SiMo_{12}$}

Again, the reaction inside the cuvette remained the same but 0.05mL additions of the seed were injected at the incrementally increased concentrations. Upon addition of the preformed {$SiMo_{12}$}, an increased formation rate was observed at the beginning of the reaction, leading to the elimination of the lag period (figure 26) and kinetic saturation of the system upon addition of $9.12x10^{-7}$ M of preformed {$SiMo_{12}$} (figure 27) providing further support that this member of Keggin species also catalyzes its own formation via a template mediated process.

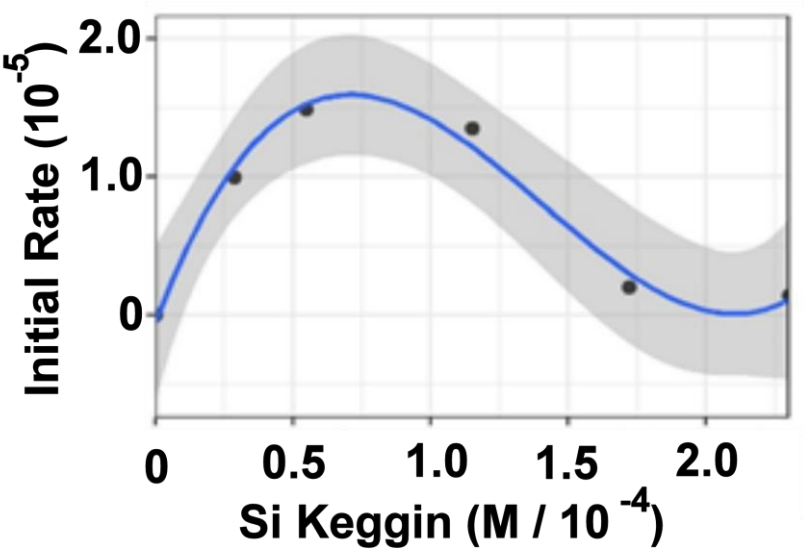

Figure 28 Kinetic saturation of {$AsMo_{12}$} autocatalyst. Formation rate vs. concentration of {$AsMo_{12}$} (Cx10-5 M) injected in the reaction mixture (in H2O at 5 °C). The experimental data points represent the initial rate of the system. An increase is observed at the beginning before reaching a plateau (saturation).

3.2.6 Concentration Variation Experiments

Additionally, we embarked on further exploring the observed incubation periods seen during the formation of the Keggin species. More specifically, we explored the effect of the concentration on the length of the observed lag time. The decrease in concentration produced an increase in the length of the incubation period for both Keggin species. In the case of {$AsMo_{12}$}, the lag time increased from roughly 180 seconds to roughly 900 seconds when decreasing the concentration by an order of magnitude. Similarly, in the case of {$SiMO_{12}$}, the lag time increased from roughly 130 seconds to roughly 380 seconds when also reducing the initial concentrations of molybdenum by an order of magnitude.

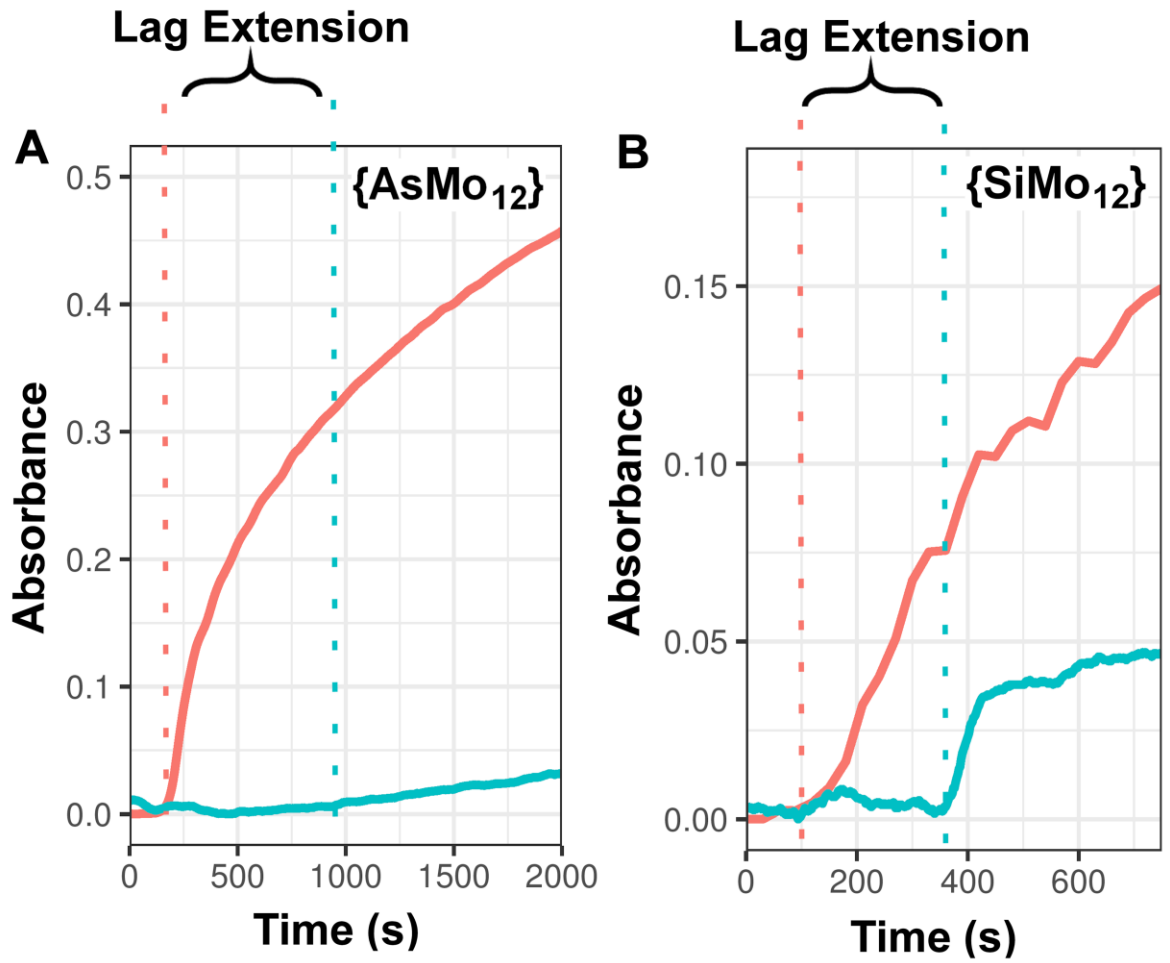

Figure 29 Representation of the effect of the [Mo] on the induction period for: A {AsMo12} and B {SiMo12}, respectively. Colour code: light blue, [Mo] = 3 x 10^{-4}; light red, [Mo] = 3 x 10^{-3}.

3.2.7 Mass Spectrometry Experiments

Another important point that required clarification in our effort to shed light upon the formation mechanism of the Keggin family members, was the fundamental species that are involved in the detected autocatalytic set. In order to achieve this, we employed electrospray ionization mass spectrometry (ESI-MS) and detected the species that are present in the reaction mixture upon mixing of the starting materials (t = 0) and after 16 hrs. Interestingly, at t = 0 the only species that are detectable were singly charged $\{Mo_2\}$ units such as $[Mo_2O_7H]^-$, $[Mo_2O_7Na(H_2O)_4]^-$, $[Mo_2O_7Na(H_2O)_5]^-$ and $[Mo^{VI}_2O_9Na_3(H_2O)_3H_2]^-$ centered at 304.78, 400.76, 416.78 and 460.78 m/z, singly charged $\{Mo_3\}$ unit, $[Mo^{V}Mo^{IV}_2O_9Na_2H_2]^-$ centered at 478.76 m/z and amounts of $\{AsMo_3\}$ units such as $[Mo^{VI}_3O_9(AsO_4)Na_2(H_2O)]^-$, $[Mo^{VI}_3O_{10}(AsO_4)Na_4(H_2O)]^-$ and $[Mo^{VI}_3O_{10}(AsO_4)Na_4(H_2O)_3]^-$ centered at 634.49, 696.76 and 732.60 m/z respectively. After 16 hrs, solution studies revealed the presence of $\{AsMo_3\}$

units and the doubly charged $[AsMo^{VI}_{11}Mo^{V}O_{39}H]^{2-}$ Keggin anion centered at 925.75 m/z value.

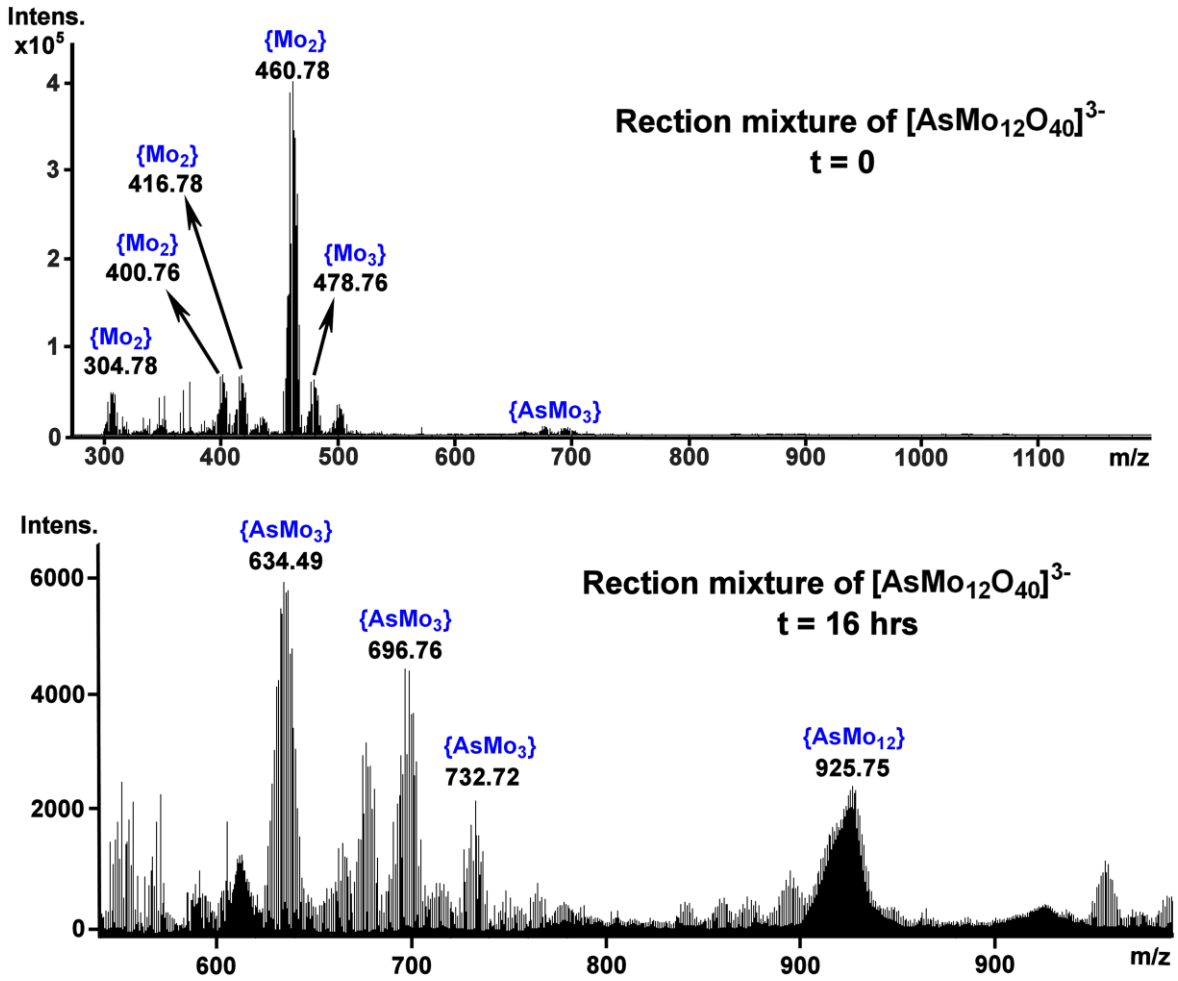

Figure 30 Negative mode electrospray ionization mass spectrum (ESI-MS) of the {AsMo12} reaction mixture in H2O at t = 0 hrs (TOP) and t = 16 hrs (BOTTOM).

This was also the case for the $\{SiMo_{12}\}$, where the ESI-MS showed that the only species visible at the start of the reaction were singly charged $\{Mo_2\}$ units such as $[Mo_2O_8(H_2O)_4H_3]^-$ and $[Mo_2O_9Na_3(H_2O)_3H_2]^-$ centered at 394.83, and 460.70 m/z, singly charged $\{SiO_4\}_x$ unit, $[(SiO_4)_3Na_2(H_2O)_2H_9]^-$ centered at 366.94 m/z and amounts of $\{SiMo_3\}$ units such as $[Mo^{V}Mo^{VI}_2O_8(SiO_4)Na_2(H_2O)]^-$ centered at 571.60 m/z respectively.

However, after roughly 16 hours, although not very present in the ESI-MS spectrum, ion mobility MS showed the presence of {$SiMo_{12}$} after 16 hours (figure 31).

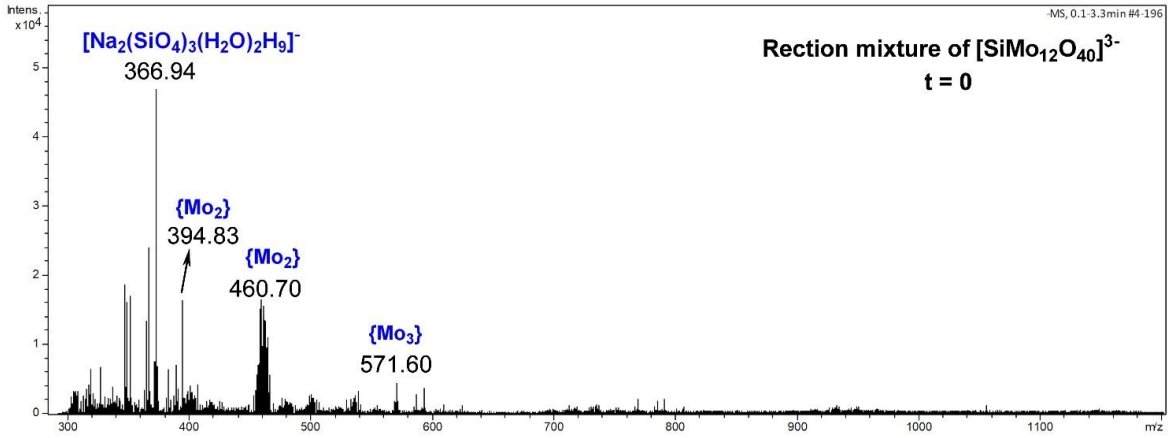

Figure 31 Negative mode electrospray ionization mass spectrum (ESI-MS) of the {SiMo12} reaction mixture in H2O at t = 0 hrs

The mass spectrometry performed reaffirms the notion that there are only small, charged dimer or trimer units at the very early stages of the self-assembly process and that there are no high nuclearity species forming at the early stages that could be influencing the beginning of the reaction and the autocatalytic pathway. This also helps to support the hypothesized model of figure 32A and validates the assumptions that the rapid formation of XMo_{12} species is directly driven by the assembly of Mo_3 and XMo_3 units.

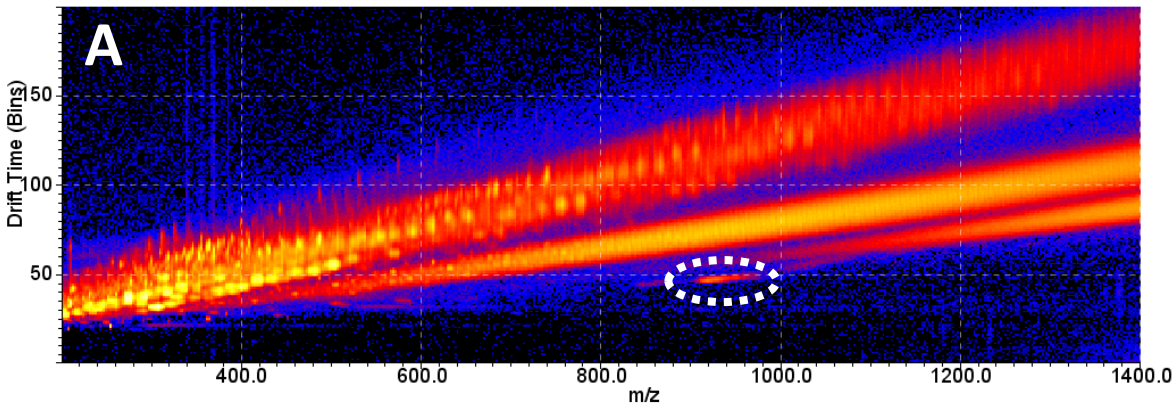

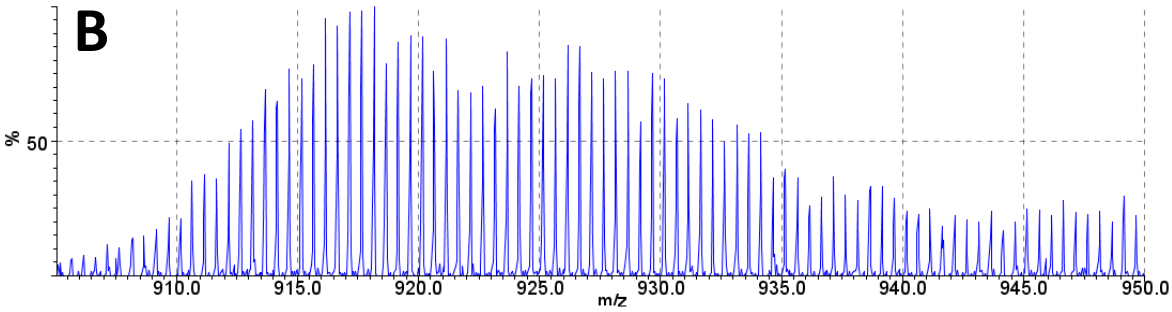

Figure 32 (A) IM-MS (-ve ion mode) mobiligram of $SiMo_{12}$, showing drift time vs m/z. Dashed ellipse shows where $SiMo_{12}$ ion can be seen. **(B)** Zoomed MS spectrum at highlighted region showing ion with m/z of around 915 at charge 2, corresponding to $SiMo_{12}$.

3.3 Computational Model

Based on the above observations, it is quite intriguing that all members of the Keggin family exhibit autocatalytic traits. However, the autocatalytic behavior is markedly different. This is potentially due to the interplay between the size and overall negative charge of the $\{XO_4\}$ (X = P, Si, As) anionic templates. The bigger size and larger overall negative charge of the $\{XO_4\}$ template, seems to slow down the autocatalytic cycle. It is also interesting that autocatalytic processes constitute a favorable resource for the formation of smaller nuclearity molecular metal oxides and its manifestation does not depend on the type of the heteroatom. However, the rate of the autocatalytic cycle can be manipulated and is directly related to the size and charge of the heteroatom.

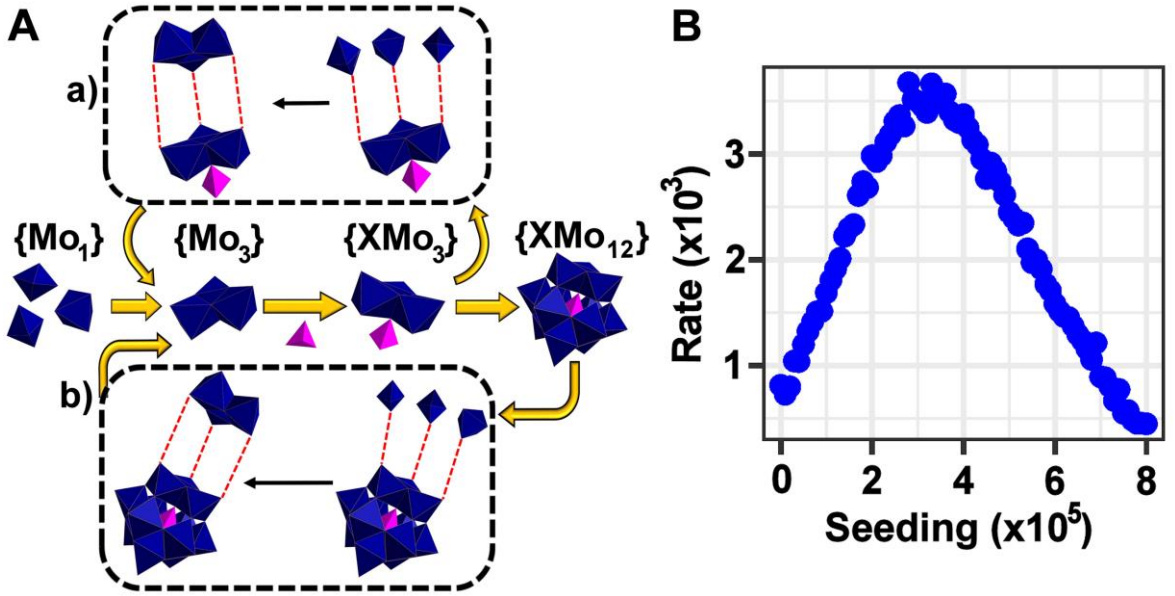

Figure 32 (A) Hypothesized embedded autocatalytic cycles. a) The final {XMo_{12}} Keggin product and the {XMo_3} subunit are responsible for the templating of more {Mo_3} building blocks. b) The subsequent templating of more {Mo3} subunits allow for an exponential production of the {XMo_{12}} Keggin. **(B)** A dynamic model of the reaction pathway hypothesized in Figure 32A is consistent with the observed kinetic saturation. Details of the model can be found in the experimental section

A consistent feature of the dynamics here, for all of the {PMo_{12}}, {$AsMo_{12}$} and {$SiMo_{12}$} clusters, is the observation of the kinetic saturation of the initial rate upon seeding. To better understand the dynamics behind this phenomenon, we implemented a computational model of the proposed reaction pathway based on the evidence provided by the conducted solution studies using temperature-controlled UV-vis and ESI-MS at different time intervals. Briefly, in this model all reactions proceed as either bimolecular or unimolecular reactions. This means that, for example, the formation of the {Mo_3} building block from molybdate is occurs in two steps with an {Mo_2} intermediate, which can degrade back into molybdate or further reactions with other molybdate to form {Mo_3}. We model the template catalysis of species by including a reaction where a molybdate can first attach to the template surface, and then proceed to add more molybdate in a step wise fashion, each step of which is reversible. We included both {XMo_3} and {XMo_{12}} as templates for the formation of {Mo_3}, as hypothesized in Figure 32A. Using this model, we explored the effect of increasing the initial amount of {XMo_{12}}, the results are shown in Figure 32B.

The model is consistent with the kinetic saturation seen in the physical experiments and can be explained by the template mechanism. When the initial amount of the template is low relative to the amount of molybdate, templates accelerate the formation of $\{Mo_3\}$ which is then used in reactions to form the $\{XMo_{12}\}$ template, thus adding more $\{XMo_3\}$ which subsequently increases this rate. This is true until the number of template surfaces becomes too large for the initial amount of molybdate. At that point, individual molybdates attach to templates but are unlikely to react with other molybdates (because they are themselves attached to templates), this means the net formation of the $\{XMo_{12}\}$ is reduced because of the time required for the unreacted molybdate to dissociate from the template and reaction with other template complexes. The fact that both the $\{XMo_3\}$ and $\{XMo_{12}\}$ can serve as templates by bringing together 3 x $\{Mo_1\}$ to form additional $\{Mo_3\}$ building blocks and finally Keggin species, means that the amount of $\{XMo_{12}\}$ at which this happens is much lower than the initial amount of molybdate.

3.4 Discussion and Conclusion

In conclusion, we identified the presence of autocatalytic traits in the formation of the Keggin family of polyoxometalate species relating to $\{AsMo_{12}\}$ and $\{SiMo_{12}\}$. Real-time monitoring UV/Vis studies have shown that the formation of Keggin species proceeds via a templated autocatalytic mechanism exhibiting an early uncatalyzed stage leading to an incubation period of ~200 seconds, as well as kinetic saturation effects in the presence of pre-formed catalyst, confirming the presence of an embedded autocatalytic cycle and an underlying molecular template process. Another interesting observation is the influence of the heteroatom on the autocatalytic cycle of the Keggin species. More specifically, there is an interplay between ionic radius the overall charge on the $\{XO_4\}^{n-}$ central component and the operational rate of the autocatalytic cycle. The higher overall charge and smaller ionic radius seems to be beneficial for the operation rate of the autocatalytic cycle. The $\{As^{V}O_4\}^{3-}$ templated Keggin appears to form at faster rates than the $\{Si^{IV}O_4\}^{2-}$ even though it possesses larger ionic radius. In the case of $\{P^{V}O_4\}^{3-}$ (reported previously) which carries the same charge but smaller than the $\{As^{V}O_4\}^{3-}$, this appears to be considerably faster among the investigated $\{XO_4\}^{n-}$ templated species. Finally, the unveiled knowledge and embedded processes within this family of inorganic clusters, provides crucial evidence for the deeper understanding of the underlying chemical processes usually vaguely described as “self-assembly”. Most importantly, this observation not only contributes to the better understanding of the masked chemical processes but also can be extrapolated and used

constructively for the discovery of new forms of materials. The underlying processes can now be manipulated at the molecular level and be used as functional modules the design of extended and interactive chemical operations where the outcome is determined by the combination of modules used.

3.5 Future Work

Here, we have successfully identified an underlying autocatalytic process in the formation of molybdenum Keggin based structures. We have shown that upon increased temperature, and therefore reaction rate, the lag period and uncatalyzed pathway is mitigated to a point where it can't be seen. We have also shown that seeding their formation with preformed Keggin allows for the elimination of an uncatalyzed pathway and the reaction rate increases from the start and shows no incubation. Finally, we have confirmed these observations with the help of a stochastic kinetic model and shows that the kinetic saturation is consistent with the physical experiments and can be explained by the template mechanism. The knowledge of that these systems behave autocatalytically could be the next step into improving or expanding syntheses of POMs.

The understanding of the kinetics and mechanisms ongoing in a chemical reaction is vital and its importance cannot be understated. It is the very basis of chemistry and only by understanding this can we target specific molecules and structures, and this is indeed the case for polyoxometalates, too. Knowing how these reactions proceed from the start can be extrapolated and used as a basis for the design of new and larger polyoxometalate clusters.

In the future, work continuing from this would involve looking at other small clusters, such as the Wells-Dawson or Anderson structures and investigate their formation, as they are very similar to the Keggin in regard to their extreme stability and ease of formation. Expanding this methodology to larger clusters however would be increasingly difficult via UV/Vis spectroscopy, as the number of different species involved in the formation of giant clusters would be difficult to determine structurally. On the other hand, further work on the computational model could show the most likely reaction pathways and this may be able to be backed up by further experimental analysis, most likely ion mobility mass spectrometry.

4 Improving the Synthesis of Mo_{368}

As discussed previously, the synthesis of high quality, single crystals of Mo_{368} is yet to be achieved. This is most likely due to the size and unique facets that the crystal possesses, such as a high number of different building blocks and a symmetry-breaking architecture that alternates from a positive to negative curvature along the surface. This is highly unusual in POMs as many of them tend to be highly symmetrical and uniform in shape or building block. First, the general structure and potential templating clusters will be discussed and then lead into work carried out into improving the yield of high-quality single crystals.

4.1 The Architecture of Mo_{368}

The full formula for the biggest POM is as follows: $Na_{48}[H_xMo_{368}O_{1032}(H_2O)_{240}(SO_4)_{48}]$. ca. $1000H_2O$ and the vast number of atoms makes determination of the exact number of hydrogen atoms or crystal water molecules extremely difficult. Although made up from the same building blocks as previous POMs, such as the $\{Mo_1\}$ monomer, the $\{Mo_2\}$ dimer and the $\{Mo(Mo_5)\}$ pentagonal unit, the Mo_{368} is unique in a way that no other derivatives or similar structures have been reported. Usually, as in the case of the wheel and ball type structures, many different types of POM exist, with a range of atom number and size but this isn't seen for the Mo_{368} which makes it truly individual and consequentially of high interest to any POM chemist.

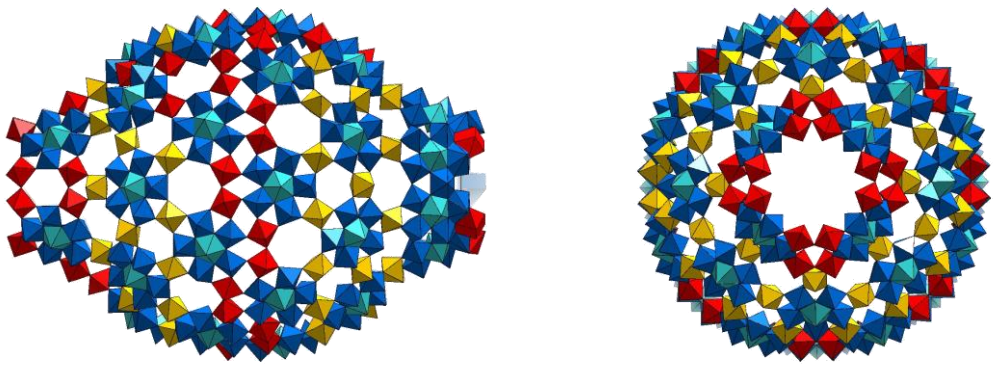

Figure 33 Polyhedral representation of the $\{Mo_{368}\}$ giant "blue lemon" structure. (Colour scheme: Pentagonal $\{Mo_6\}$ units = blue, dimer $\{Mo_2\}$ units = red, monomer $\{Mo_1\}$ units = yellow).

Of the 268 molybdenum centres, 112 of them are in a reduced Mo^{V} state while the remaining 256 remain in the Mo^{VI} oxidation state, resulting in 30.5% of the structure being reduced. This is much higher than its wheel counterparts (the Mo_{154} is only ~18% reduced) but the syntheses are very similar. However, the Mo_{368} is highly specific in its formation and only specific reaction conditions will obtain it. One specific condition is the abundance of SO_4^{2-} ligands and these are of high importance. The myriad of sulphate ions not only prevents uncontrolled linking but also allows for initial protonation in order to establish any linking in the first place. However, this does not occur when acids such as HCl or $HClO_4$ are used to provide Cl^- or ClO_4^- ions, as they are much weaker at coordinating and instead wheel-type structures will be formed. On the other hand, SO_4^{2-} also provides a coordination that isn't too strong as in the case of PO_4^{3-}, which would only form Keggin based structures. Therefore, the use of sulphuric acid is very specific to ensure a coordination with the building blocks in a way that only results in the formation of Mo_{368}.

The structure can be described as being composed of an amalgamation of two smaller structures: a central $\{Mo_{176}\}$ unit capped by two $\{Mo_{102}\}$ units. The $\{Mo_{176}\}$ wheel-type structure can be broken down into 16 $\{Mo_{11}\}$ building units and removal of a single $\{Mo_1\}$ monomer produces a $\{Mo_{10}\}$ building unit which is used in the central band. The $\{Mo_{102}\}$ Keplerate ball-type structure can be broken down into several $\{Mo_{11}\}$ building units and these are used in the capping of the structure.

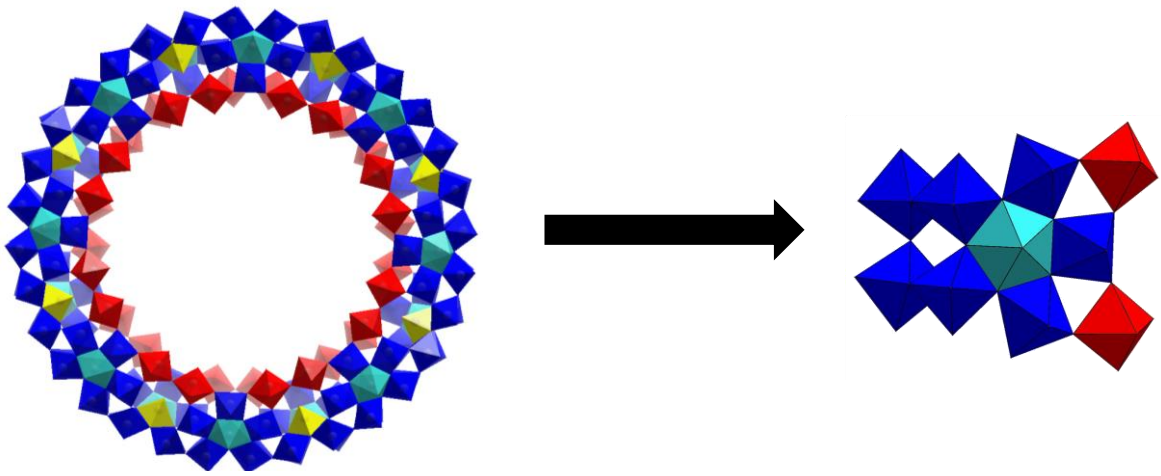

Figure 34 Polyhedral representation showing $\{Mo_{176}\}$ broken down into its $\{Mo_{10}\}$ building unit

The {Mo_{102}} is similar in structure to the first reported Keplerate in the {Mo_{132}} but instead of metal-metal bonded {Mo_2} dimers between the {$Mo(Mo_5)$} pentagonal units there is only {Mo_1} monomers bonded between these.

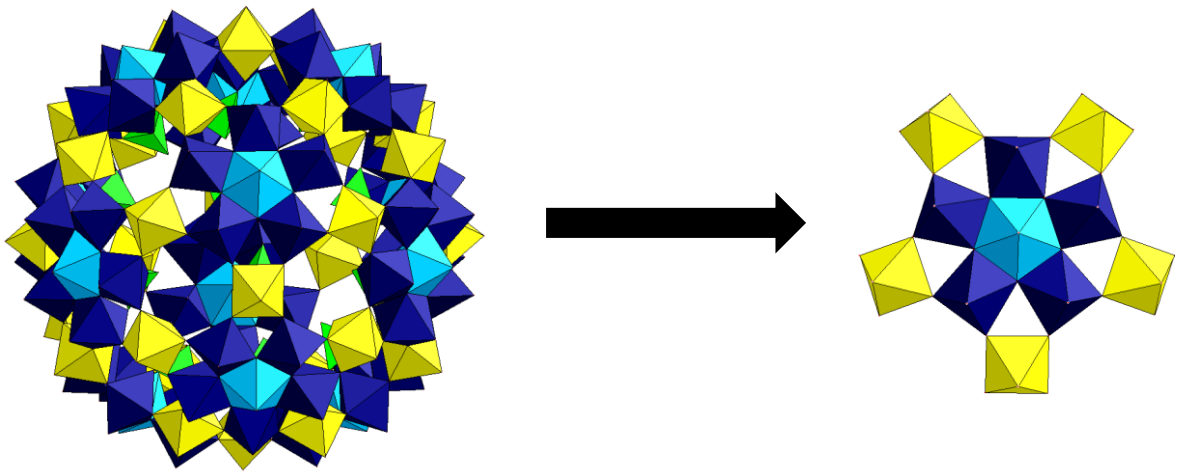

Figure 35 Polyhedral representation showing {Mo_{102}} broken down into its {Mo_{11}} building unit

4.2 The Synthesis of Mo_{368}

The following synthesis was first one reported in 2002 and is the only reported synthesis that allows for the formation of single crystals of Mo_{368}:

$Na_2S_2O_4$ (0.15 g, 0.86 mmol) as reducing agent was added to a stirred solution of Na_2MoO_4 .$2H_2O$ (3 g, 12.4 mmol) in water (10 mL) which was acidified with 0.5M H_2SO_4 (35 mL; immediate color change to blue).

This is taken from reference 18 and they state that they obtained 0.8mg of crystals when collected by filtration. However, when performing this reaction, almost every time, a very large amount of amorphous precipitate is formed while only producing a small number of single crystals, if any at all. This amorphous powder is almost impossible to determine analytically and so the goal was set to improve the synthesis to only obtain single crystals of Mo_{368}.

To do this, a robotic platform was used for rapid cluster synthesis. The design of this platform was achieved by another group member and full details regarding its hardware and software can be found at reference [118]. The platform incorporated the use of a Geneva wheel to position reaction vials below a series of peristaltic pumps and allowed for 24 reactions to be done at a ~14mL capacity.

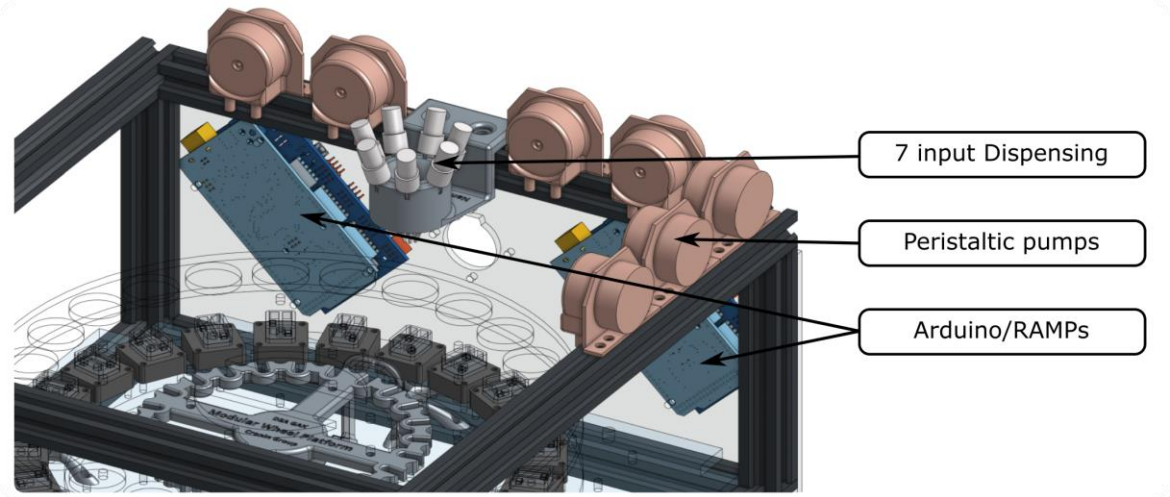

Figure 36 Image showing pumps, control boards and dispensers. Taken from reference 119 with permission.

Whereas previously the use of this robotic platform involved collating the data and inputting it into an algorithm so machine learning could aid prediction of compound reactivity, all of the data and crystals produced were analyzed by hand and the reaction conditions adjusted personally. The first step in improving the synthesis is confirming that the product can be synthesized in the first place and so the reaction conditions laid out previously *via* reference 18 were scaled accordingly, making sure to keep the ratio of reactants the same. All concentration ratios were normalized to the concentration of the reducing agent, as this is the reactant with the lowest concentration. Also, the concentration of molybdate was kept to that of the original literature concentration, 1.24M, in order to make a better comparison. As the robotic platform is only able to perform liquid handling, each of the three reactants used in the literature reaction conditions were made up to the following concentrations – $Na_2MoO_4.2H_2O$ to 1.24M as stated before, $Na_2S_2O_4$ to 0.5M and H_2SO_4 to 0.5M. When looking at the literature reaction conditions, the molar ratio of Mo:$Na_2S_2O_4$: H_2SO_4 in these concentrations is 10.74:1:11.06 respectively. Using these molar concentrations, the volume

ratio when using the above concentrations is 2.37:0.547:6.06 and so this reaction was performed on the robotic platform initially. Concurrently with this, exploration of the surrounding chemical space was performed. Any crystals obtained were checked using X-ray crystallography but only a unit cell match was needed to know if the Mo_{368} was found. However, the Mo_{368} also has a very distinctive crystal shape that can be described as an elongated benzene type shape. Therefore, as the robot runs went on, in order to improve output and speed up the process, only the specific crystal shape was necessary to observe, and subsequent runs were directed towards chemical conditions that obtained this specific crystal shape.

Run	***Na_2MoO_4***	***$Na_2S_2O_4$***	***H_2SO_4***	***Result***
1	2.37	0.547435	6.0566	No crystals
2	2.37	0.547435	6.0566	No crystals
3	2.37	0.547435	6.0566	No crystals
4	2.37	0.547435	6.0566	No crystals
5	2.37	0.273718	6.0566	No crystals
6	2.37	0.359321	6.0566	No crystals
7	2.37	0.444925	6.0566	No crystals
8	2.37	0.530528	6.0566	No crystals
9	2.37	0.616132	6.0566	No crystals
10	2.37	0.701735	6.0566	No crystals
11	2.37	0.757339	6.0566	No crystals
12	2.37	0.872942	6.0566	No crystals
13	2.37	0.958546	6.0566	No crystals
14	2.37	1.044149	6.0566	No crystals
15	2.37	0.547435	3.0566	No crystals
16	2.37	0.547435	4.0566	No crystals
17	2.37	0.547435	5.0566	No crystals
18	2.37	0.547435	6.0566	No crystals
19	2.37	0.547435	7.0566	Amorphous precipitate
20	2.37	0.547435	8.0566	**Mo368**
21	2.37	0.547435	9.0566	**Mo368**
22	2.37	0.547435	10.0566	**Mo368 (best crystal)**
23	2.37	0.547435	11.0566	Rod shaped Crystals
24	2.37	0.547435	12.0566	Amorphous precipitate
Totals	56.88	14.22342	160.3584	

Figure 37 First robotic platform run showing amounts added in mL using the previously stated concentrations and the results in the last column.

As can be seen in figure 33, using the literature molar ratios, no Mo_{368} crystals were obtained. This was repeated many times and failed to obtain the desired product every time. However, when the ratio of sulfuric acid is increased from 6 to between 8.05-10.05, Mo_{368} was obtained. A slightly higher ratio of 11.05 obtained a sort of rod-shaped crystal that was also targeted in subsequent runs, as the diffraction of this crystal was always poor, and its composition is still a mystery. After finding that a higher concentration of sulfuric acid was needed, runs were undertaken to find the optimal amount of reducing agent.

Run	Na_2MoO_4	$Na_2S_2O_4$	H_2SO_4	
1	2.37	0.25	9.5	No crystals
2	2.37	0.3	9.5	No crystals
3	2.37	0.35	9.5	**Small Mo368 crystals**
4	2.37	0.4	9.5	**Small Mo368 crystals**
5	2.37	0.45	9.5	**Small Mo368 crystals**
6	2.37	0.5	9.5	**Small Mo368 crystals, Mo102 crystals**
7	2.37	0.55	9.5	Rod shaped crystals
8	2.37	0.6	9.5	Rod shaped crystals
9	2.37	0.65	9.5	Rod shaped crystals
10	2.37	0.7	9.5	Small rod-shaped crystals
11	2.37	0.75	9.5	Small rod-shaped crystals
12	2.37	0.8	9.5	amorphous precipitate
13	2.37	0.85	9.5	amorphous precipitate
14	2.37	0.9	9.5	amorphous precipitate
15	2.37	0.95	9.5	amorphous precipitate
16	2.37	1	9.5	amorphous precipitate
17	2.37	1.05	9.5	amorphous precipitate
18	2.37	1.1	9.5	amorphous precipitate
19	2.37	1.15	9.5	amorphous precipitate
20	2.37	1.2	9.5	amorphous precipitate
21	2.37	1.25	9.5	amorphous precipitate
22	2.37	1.3	9.5	amorphous precipitate
23	2.37	1.35	9.5	amorphous precipitate
24	2.37	1.4	9.5	amorphous precipitate
Totals	56.88	19.8	228	

Figure 38 Robotic platform run varying reducing agent

As can be seen in figure 34, when too much reducing agent is used, the only product obtained is amorphous precipitate. Lower amounts of reducing agent, at a ratio between 0.35 and 0.75 obtained a variety of crystal shapes, with lower amount producing Mo_{386} and larger amounts producing the unknown rod-shaped crystals. There is also a square-shaped crystal that can be obtained, which upon further analysis is known to be the previously shown Mo_{102} Keplerate-type ball (figure 31). Synthesizing this ball reinforces the assumption that it used as a template in the Mo_{368} synthesis and would be an interesting avenue to explore further. After finding an approximate range for the optimal amount of reducing agent, this region was looked at in more detail.

Run	***Na_2MoO_4***	***$Na_2S_2O_4$***	***H_2SO_4***	***Result***
1	2.37	0.4	9.5	Small amount of Mo102
2	2.37	0.415	9.5	
3	2.37	0.43	9.5	
4	2.37	0.445	9.5	
5	2.37	0.46	9.5	Mo102 (best crystals)
6	2.37	0.475	9.5	
7	2.37	0.49	9.5	
8	2.37	0.505	9.5	
9	2.37	0.52	9.5	**Small Mo368 crystals**
10	2.37	0.535	9.5	**Small Mo368 crystals**
11	2.37	0.55	9.5	**Small Mo368 crystals**
12	2.37	0.565	9.5	**Small Mo368 crystals**
13	2.37	0.58	9.5	**Small Mo368 crystals**
14	2.37	0.595	9.5	
15	2.37	0.61	9.5	Rod shaped crystals
16	2.37	0.625	9.5	Rod shaped crystals
17	2.37	0.64	9.5	Rod shaped crystals
18	2.37	0.655	9.5	Rod shaped crystals
19	2.37	0.67	9.5	Rod shaped crystals
20	2.37	0.685	9.5	
21	2.37	0.7	9.5	Small rod-shaped crystals, Mo102 crystals
22	2.37	0.715	9.5	Small rod-shaped crystals, Mo102 crystals
23	2.37	0.73	9.5	Small rod-shaped crystals, Mo102 crystals
24	2.37	0.745	9.5	Small rod-shaped crystals, Mo102 crystals
Totals	56.88	13.74	228	

Figure 39 Robotic platform run varying reducing agent again

Figure 35 shows that within the range of 0.4-0.75 ratio of reducing agent, a pattern can be seen. Lower amounts of reducing agent produce the square shaped Mo_{102}, then an increase produces Mo_{368}, and a further increase produces the unknown rod-shaped crystals. When looking at the molar ratios, as stated previously, the literature molar ratio of Mo : $Na_2S_2O_4$: H_2SO_4 is 10.74:1:11.06 respectively. However, after running over 300 runs on the robotic platform, we found that the ratio with the most success in obtaining single crystals of Mo_{368} is actually 10.9:1:17.3. This is an increase in ratio of both the molybdate and acid and although may not seem like much, the synthesis of POMs drastically can change upon even the smallest of reaction condition alterations.

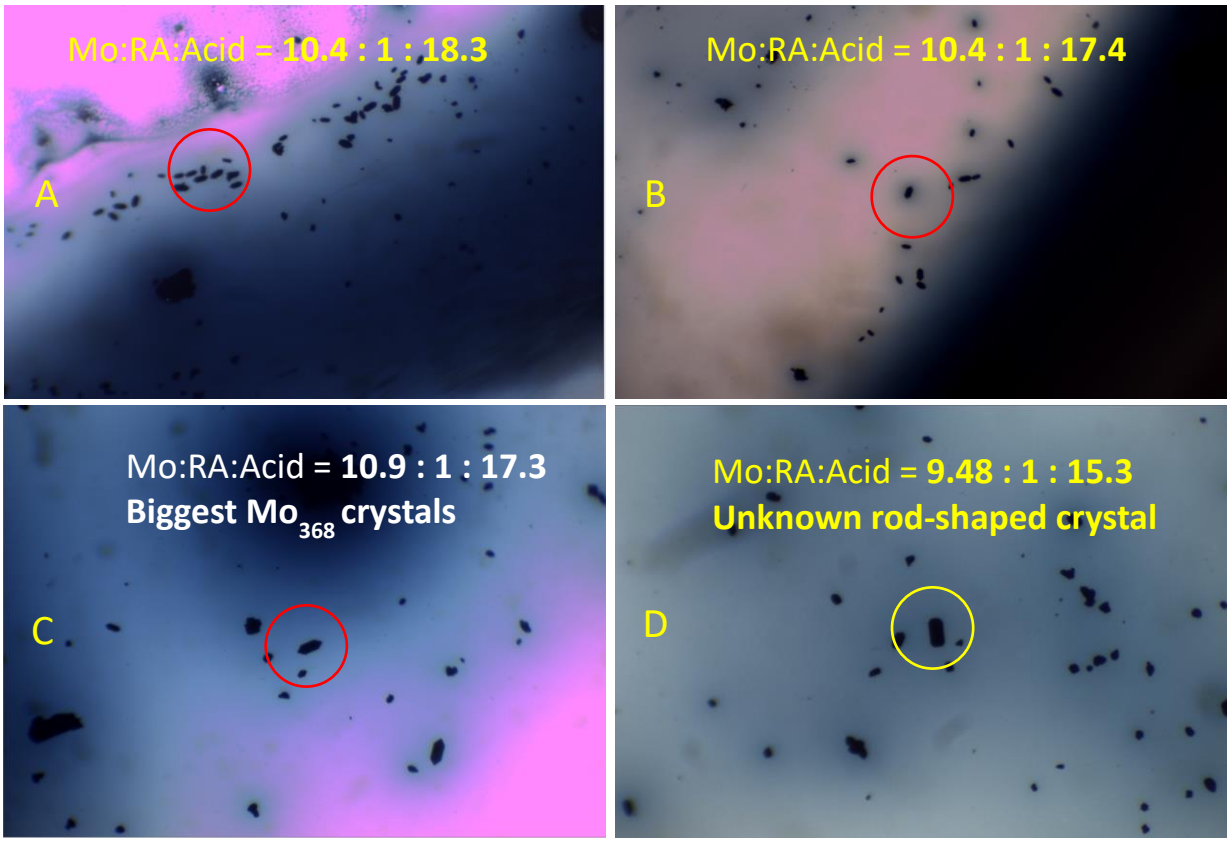

Figure 40 Microscope pictures of crystals obtained from robotic platform runs. **A** and **B** show the unique crystal shape of Mo_{368}, while **C** shows the best obtained crystals of Mo_{368} and **D** shows unknown rod-shaped crystals

Figure 37 shows the successful acquisition of single crystals of Mo_{368} and also the crystals of the unknown rod-shapes that were obtained at higher reducing agent concentrations. The crystals of Mo_{368} were usually only good enough to obtain a correct unit cell but wouldn't produce a good enough diffraction for a complete data set, but again, the unique crystal shape is a good confirmation to target initially. The square shaped crystals can also be seen in figure 38.

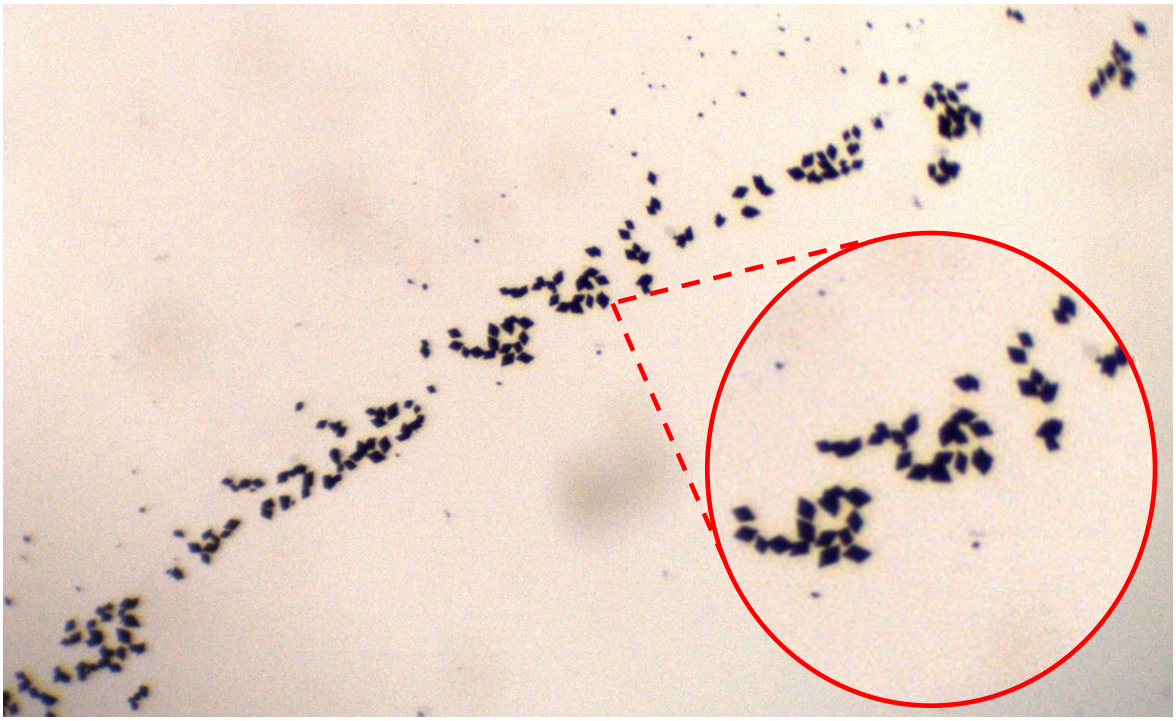

Figure 41 Microscope pictures of the square/rhomboid shaped crystals of Mo_{102} that were obtained on the robotic platform.

As so many robot runs were done, it is difficult to keep up with the vast number of results and a better way to compare is to visualize the chemical space on a graph. From the robot runs we found there are 6 different possible outcomes when performing these syntheses. The seven different product outcomes are:

1. Square/Rhomboid-shaped crystals (Figure 37)
2. Mo_{368} (Figure 36A/B/C)
3. A mixture of Mo_{368} and square-shaped crystals
4. Rod-shaped crystals (Figure 37D)

5. A mixture of rod-shaped and square-shaped crystals

6. Nothing/amorphous precipitate

Plotting out these results on a graph that is normalized to the concentration of molybdate provides figure 38, with the X-axis showing the ratio of H_2SO_4 to molybdate and the Y-axis showing the ratio of reducing agent to molybdate.

As can be seen from figure 39, all of the robot runs that obtained any kind of crystal all did so at a much higher concentration of acid when compared to the literature synthesis and the ratio of acid to molybdate looks to range between 1.3-1.9:1, Also, the concentration of reducing agent to molybdate looks to range from 0.06-0.13:1. This graph shows a very clear window of chemical space in which successful crystal synthesis can be achieved. Also looking at the graph, there is a point at which the concentration of reducing agent shifts from producing square shaped Mo_{102} to the unknown rod-shaped crystals. Determination of these unknown crystals is the most important step in understanding what kinetic or mechanistic change is happening.

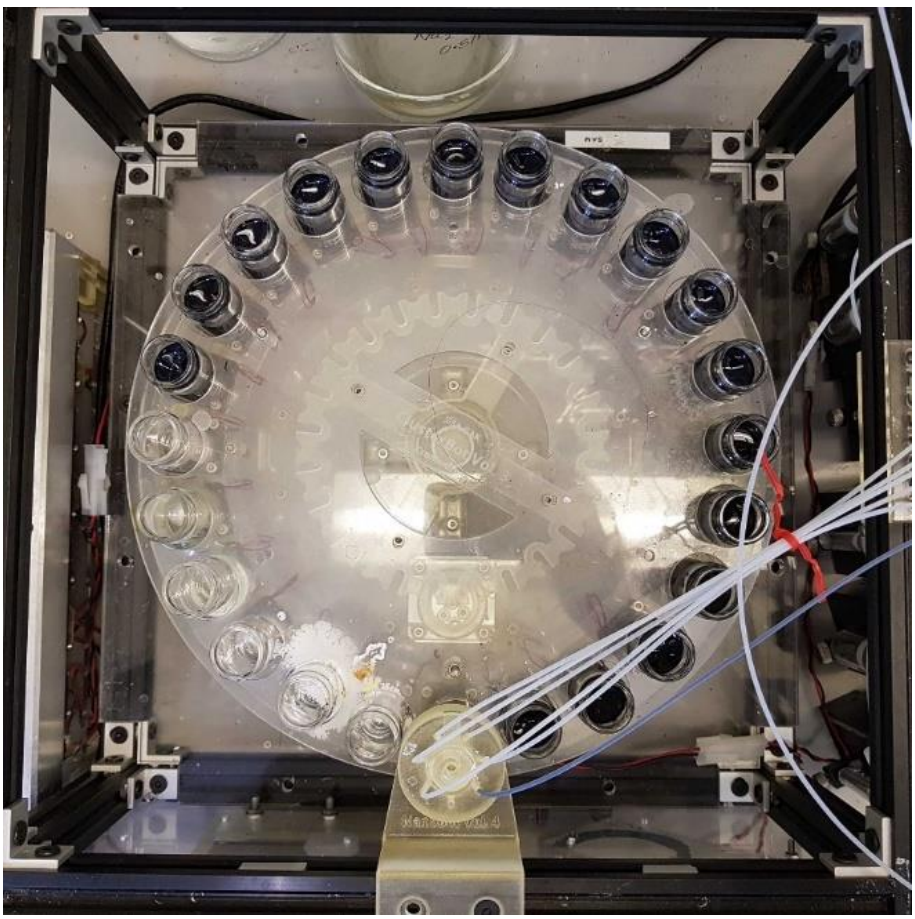

Figure 42 Picture of the robotic platform during a run of Mo_{368} synthesis

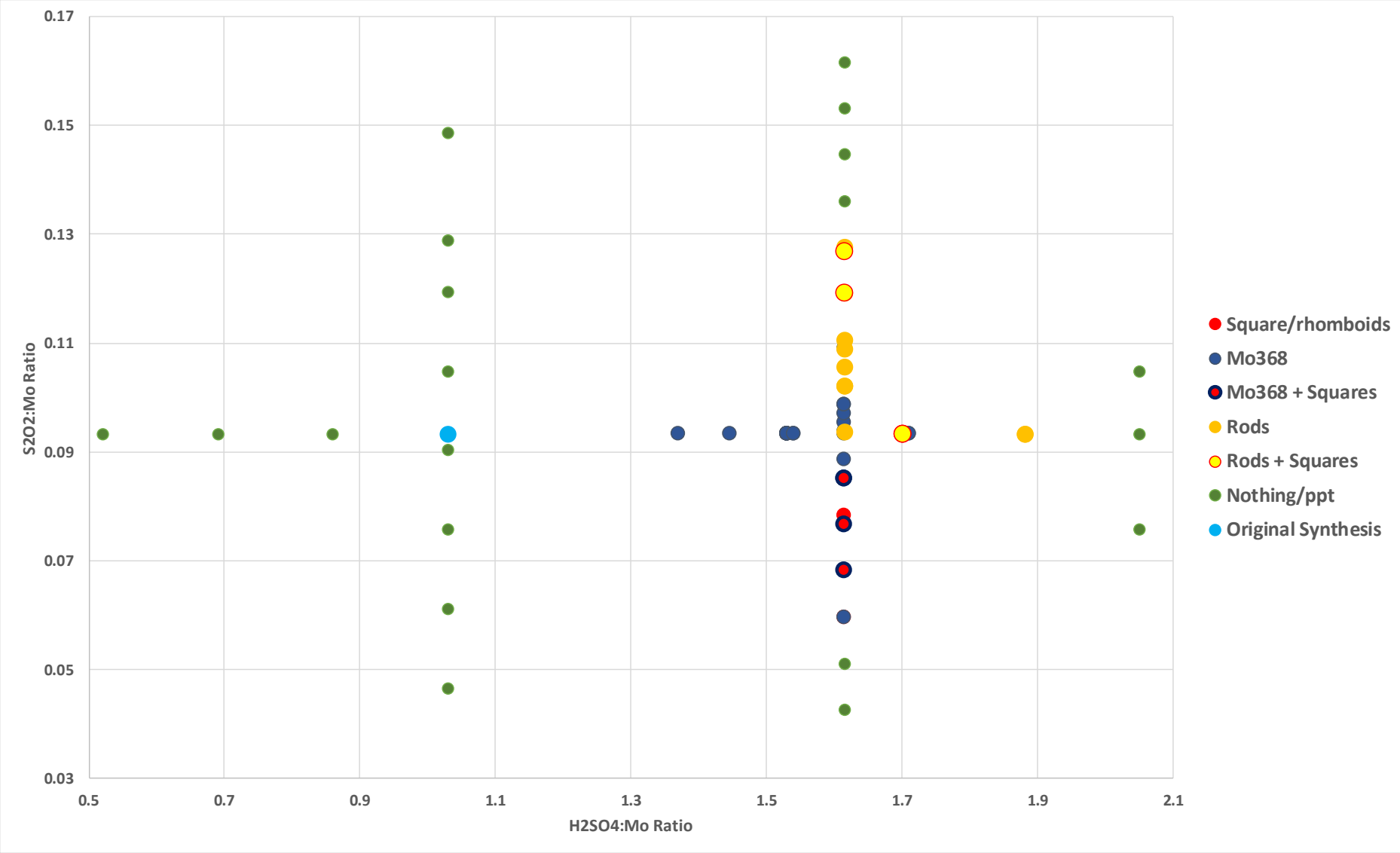

Figure 43 Graph showing plotted chemical space found using the robotic platform. The light blue point is the original literature synthesis

4.3 Conclusions and Future Work

The repeatable synthesis of high-quality single crystals of the largest POM known is still something that hasn't been achieved after more than two decades since its first publication. Employing the use of a robotic platform for liquid handling and chemical synthesis allowed for rapid output of reactions to allow the chemical space surrounding this synthesis to be explored.

The synthesis of Mo_{368} single crystals was found to occur at a higher acid concentration than previously reported, although the crystal quality still wasn't good enough for full X-ray diffraction and other elemental analyses. It was also always surrounded by small amounts of precipitate and subsequent runs would look to improve it even further to remove as much precipitate as possible and form higher quality crystals. Along with the Mo_{368}, the synthesis of Mo_{102} Keplerate-type balls was also discovered, although this is a reported structure. Finally, the synthesis of an unknown rod-shaped crystal was seen, and it is still not clear what this is as the diffraction is always poor. Any subsequent runs would also target this rod-shaped crystal and its structural determination is one of the most important follow ups to this project.

Due to time constraints and other uncontrollable factors, focus on this project shifted elsewhere and no more robot runs to explore the chemical space have been carried out. However, looking at figure 40, there are four clear areas where the chemical space should be looked at in order to ascertain the whole picture as to how the ratio of reducing agent and acid to molybdenum affects the synthesis of Mo_{368}.

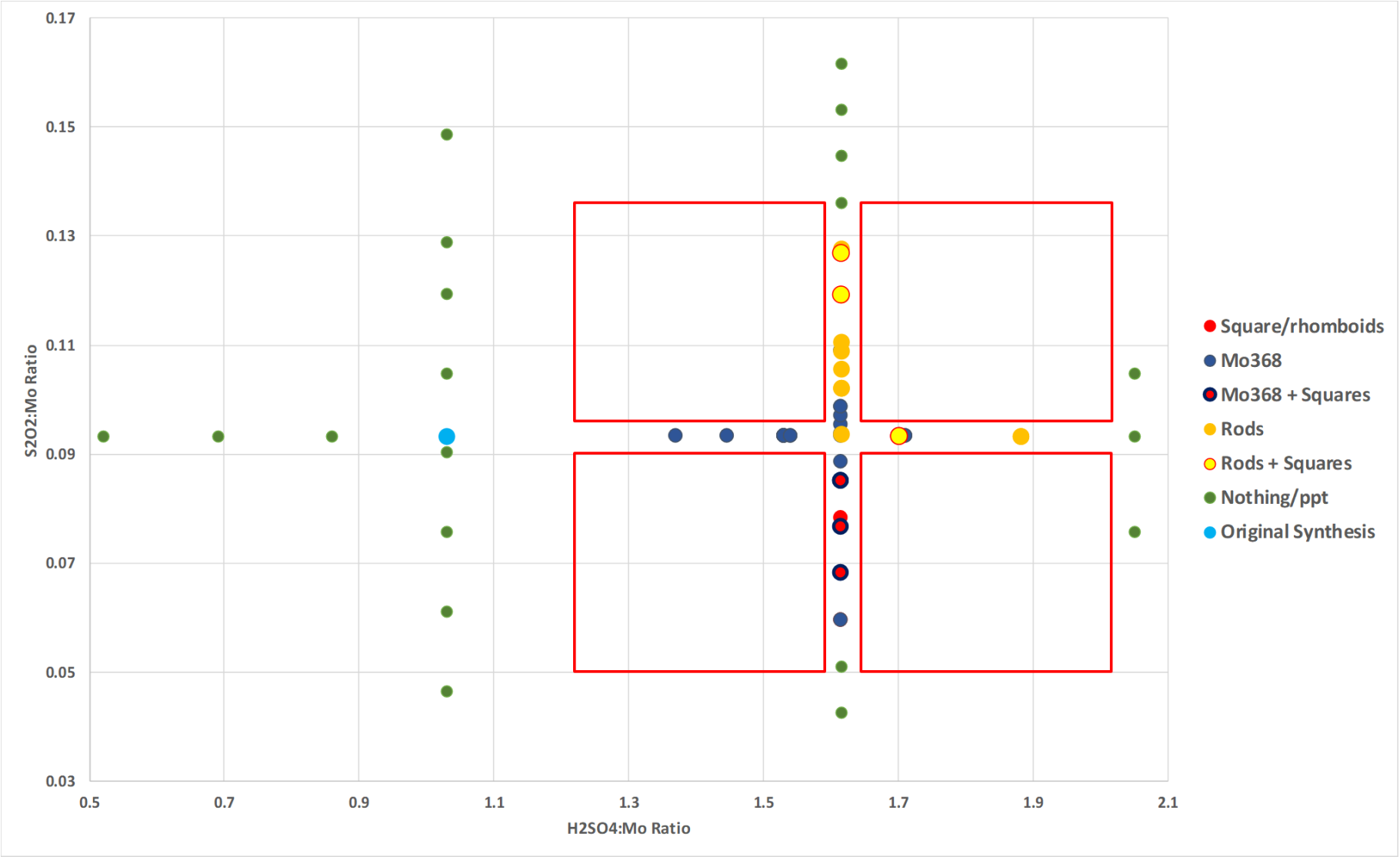

Figure 44 Graph highlighting the four areas to target when further exploring the chemical space of this system

5 Experimental

5.1 Materials

All reagents and solvents were purchased from Sigma-Aldrich Chemical Company Ltd., Alfa Aesar, and Tokyo Chemical Industries. Materials were used without further purification, unless otherwise stated.

5.2 Instrumental

5.2.1 UV-Vis Spectroscopy

All analyses were performed on a JASCO V-670 UV-Vis spectrometer, fitted with a JASCO EHC-716 temperature controller under nitrogen atmosphere.

5.2.2 Single Crystal X-Ray Diffraction

A small amount of the solution containing the crystals was pipetted onto a glass slide. Any excess solvent was removed and Fombolin oil was added to the crystals. The Fombolin oil allows for easier crystal mounting onto the goniometer and also protects the crystals during mounting and cooling. Single crystal datasets or unit cells were collected at 150K either using a Bruker Apex II Quasar diffractometer equipped with a graphite monochromator (λ ($Mo_{K\alpha}$) = 0.71073Å) or a Rigaku Xta LAB Synergy diffractometer with a rotating anode MoKα source and Rigaku HyPix-Arc 150° detector. Structure solution and refinement were carried out using SHELXS-2014 and SHELXL-2014 using WINGX.

5.2.3 pH Measurements

Any pH measurements were taken on a Hanna Instruments HI-2210-02 Bench Top pH Meter with pH electrode (HI 1131B) and temperature probe (HI 7662).

5.2.4 Mass Spectrometry Monitoring

ESI-MS data was collected using a Q-trap, time-of-flight MS (Maxis Impact MS) instrument supplied by Bruker Daltonics Ltd. The detector was a time-of-flight, microchannel plate detector and all data was processed using the Bruker Daltonics Data Analysis 4.1 software,

whilst simulated isotope patterns were investigated using Bruker Isotope Pattern software and Molecular Weight Calculator 6.45. The calibration solution used was Agilent ES tuning mix solution, Recorder No. G2421A, enabling calibration between approximately 100 m/z and 3000 m/z. Samples were dissolved in H_2O and introduced into the MS via direct injection at 180 µL h -1 . The ion polarity for all MS scans recorded was negative, at 180°C, with the voltage of the capillary tip set at 4000 V, end plate offset at –500 V, funnel 1 RF at 300 Vpp and funnel 2 RF at 400 Vpp.

Ion-mobility mass-spectrometry measurements were performed on a Synapt™ G2 HDMS™ from Waters. All compounds were dissolved in water and solutions were made to roughly 20mM. The analyte solutions were filtered through a syringe filter (0.2 µm) before injected into the spectrometer via a syringe pump at a flow rate of 180 µL·min-1 . Ion-voltages were adjusted for optimum ionization in HRES-mode and kept constant for IMS-MS measurements.

5.3 Computational Model Details

To verify the hypothesized autocatalytic cycles were consistent with the observed data, we implement a computational model of the system. In this model all reactions are either unimolecular (A -> B + C) or bimolecular (A + B ->C + D). Rather than model every possible reaction and intermediate as in previous approaches (ref 36) we focused instead on verifying the kinetic saturation was consistent with the observed kinetic saturation profiles. Therefore, the model consists of the follow reactions:

$2Mo \rightarrow Mo_2$, c1

$Mo_2 \rightarrow Mo + Mo$, c2

$Mo_2 + Mo \rightarrow Mo_3$, c1

$Mo_3 \rightarrow Mo_2 + Mo$, c2

$X + Mo_3 \rightarrow XMo_3$, c3

$XMo_3 + Mo \rightarrow XMo_3[Mo]$, c4

$XMo_3[Mo] \rightarrow XMo_3 + Mo$, c5

$XMo_3[Mo] + Mo \rightarrow XMo_3[Mo_2]$, c4

$XMo_3[Mo_2] \rightarrow XMo_3[Mo] + Mo$, c5

$XMo_3[Mo_2] + Mo \rightarrow XMo_3 + Mo_3$, c4

$XMo_3 + Mo_3 \rightarrow X[Mo_3]_2$, c6

$X[Mo_3]_2 \rightarrow XMo_3 + Mo_3$, c7

$X[Mo_3]_2 + XMo_3 \rightarrow XMo_{12}$, c6

$XMo_{12} + Mo \rightarrow XMo_{12}[Mo]$, c8

$XMo_{12}[Mo] \rightarrow XMo_{12} + Mo$, c9

$XMo_{12}[Mo] + Mo \rightarrow XMo_{12}[Mo_2]$, c8

$XMo_{12}[Mo_2] \rightarrow XMo_{12}[Mo] + Mo$, c9

$XMo_{12}[Mo_2] + Mo \rightarrow XMo_{12} + Mo_3$, c8

For the results in Figure 10 the rate constants were set such that c1 = 10-6, c2 = 1.0, c3 =0.01, c4 = 10-4 , c5 = 10-5, c6 = 1.0 c7= 0.01, c8 = 0.01 c9= 0.01. Other rate constants were tried and the result hold for situations where the forward rate of Mo3 formation is faster for the templated reactions than for the spontaneous reaction. The reaction network was solved using a kinetic monte Carlo approach (Gillespie Ref, PNAS ref). Each point in Figure 10 represents the average over 100 independent runs at that seed value (error bars show the standard deviation). For all simulations the initial number of Molybdate (Mo) and hetero atoms (X) was set to 10000, the initial number of Keggin molecules was set according to the seeded amount (x-axis figure 10), all other species started with 0 concentration, all simulations were integrated for 2000 time units. The model was implemented using Julia v1.7 and the packages DifferentialEquations.jl and DiffEqBiological.jl

5.4 Monitoring of {$AsMo_{12}$} formation

To monitor the formation of {$AsMo_{12}$}, the following 3 solutions were freshly prepared prior to every measurement. Solution A: 0.02 M aqueous solution of $Na_2MoO_4 \cdot 2H_2O$ (0.5% w/v); Solution B: 0.028 M aqueous solution of ascorbic acid (0.5% w/v) and solution C: 0.575 x 10–4 M solution of $Na_2HAsO_4 \cdot 7H_2O$. Then 0.5 mL of solution A, 0.5 mL of solution B and 2 mL of solution C were mixed in the UV-vis cuvette and the UV-vis spectrum was monitored as a function of time at 800 nm using a time-course measurement programme. The temperature controller was always set to 5 ºC unless stated otherwise. To monitor the effect of seeding with preformed $AsMo_{12}$, these concentrations were diluted by a factor of 5.

5.5 Monitoring of {$SiMo_{12}$} formation

To monitor the formation of {$SiMo_{12}$}, the following 3 solutions were freshly prepared prior to every measurement. Solution A: 0.04 M aqueous solution of $Na_2MoO_4 \cdot 2H_2O$ (1% w/v); Solution B: 0.0565 M aqueous solution of ascorbic acid (0.5%w/v) and solution C: 1.15x10–3 M aqueous solution of Na_2SiO_3. Then 0.5 mL of solution A, 0.5 mL of solution B and 2 mL of solution C were added in a UV-vis cuvette and the UV-vis spectrum was monitored as a function of time at 800 nm using a time-course measurement programme. The temperature controller was always set to 5 ºC unless stated otherwise. To monitor the effect of seeding with preformed {$SiMo_{12}$}, these concentrations were diluted by a factor of 10.

5.6 Preparation of {$AsMo_{12}$} Seed

10 g $Na_2MoO_4 \cdot 2H_2O$ was dissolved in 50 mL H_2O (0.8 M) to make solution A, 10 g ascorbic acid was dissolved in 50 mL H_2O (1.13 M) to make solution B and 3g $Na_2HAsO_4.7H_2O$ was dissolved in 50 mL H_2O to make solution C (0.2M). Then, 4 mL of solution A, 4 mL of solution B and 16 mL of solution A were mixed in a 50 mL beaker for at least 24 hours. Various amounts of this combined mixture were then made up to 100mL in a volumetric flask to produce the different concentrations of {$AsMo_{12}$} seed.

5.7 Preparation of {$SiMo_{12}$} Seed

10 g $Na_2MoO_4 \cdot 2H_2O$ was dissolved in 50 mL H_2O (0.8 M) to make solution A, 10 g ascorbic acid was dissolved in 50 ml H2O (1.13 M) to make solution B and 1.22 g Na_2SiO_3 was

dissolved in 50 mL H_2O to make solution C (0.2 M). Then, 4 mL of solution A, 4 mL of solution B and 16 mL of solution A were mixed in a 50 mL beaker for at least 24 hours. Various amounts of this combined mixture were then made up to 100ml in a volumetric flask to produce the $\{SiMo_{12}\}$ seed.

6 References

1 H. Stephan, M. Kubeil, F. Emmerling and C. E. Müller, *Eur. J. Inorg. Chem.*, 2013, **2013**, 1585–1594.

2 J. M. Clemente-Juan, E. Coronado and A. Gaita-Ariñoa, *Chem. Soc. Rev.*, 2012, **41**, 7464–7478.

3 M. A. AlDamen, M. O. Sinnokrot, S. B. Atta, R. A. Al Qawasmeh and C. J. Gómez-García, *J. Struct. Chem.*, 2020, **61**, 559–565.

4 I. V. Kozhevnikov, *Chem. Rev.*, 1998, **98**, 171–198.

5 D. L. Long, E. Burkholder and L. Cronin, *Chem. Soc. Rev.*, 2007, 36, 105–121.

6 A. Proust, R. Thouvenot and P. Gouzerh, *Chem. Commun.*, 2008, 1837–1852.

7 C. W. Scheele, *Samtliche Physische und Chemische Werke*, 1793.

8 J. J. Berzelius, *Ann. Phys.*, 1826, **82**, 369–392.

9 C. Marignac, *C. R. Acad. Sci*, 1862, **55**, 888.

10 A. Rosenheim and F. Kohn, *Zeitschrift für Anorg. Chemie*, 1911, **69**, 247–260.

11 L. Pauling, *J. Am. Chem. Soc.*, 1929, **51**, 2868–2880.

12 J. F. Keggin, *Nature*, 1933, 131, 908–909.

13 J. F. Keggin, Keggin and J. F., *Proc. R. Soc. London. Ser. A, Contain. Pap. a Math. Phys. Character*, 1934, **144**, 75–100.

14 H. T. E. Jr, *The Molecular Structure of the Hexamolybdotellurate Ion in the Crystal Complex with Telluric Acid, (NH4)6ITeMo6Oz4]. Te(OH)6.7HzO*, 1974, vol. 30.

15 J. S. Anderson, *Nature*, 1937, 140, 850.

16 A. Müller, E. Krickemeyer, J. Meyer, H. Bögge, F. Peters, W. Plass, E. Diemann, S. Dillinger, F. Nonnenbruch, M. Randerath and C. Menke, *Angew. Chemie Int. Ed. English*, 1995, **34**, 2122–2124.

17 A. Müller, E. Krickemeyer, H. Bögge, M. Schmidtmann and F. Peters, *Angew. Chemie Int. Ed.*, 1998, **37**, 3359–3363.

18 A. Müller, E. Beckmann, H. Bögge, M. Schmidtmann and A. Dress, *Angew. Chemie Int. Ed.*, 2002, **41**, 1162–1167.

19 Y. P. Jeannin, *Chem. Rev.*, 1998, **98**, 51–76.

20 M. T. Pope and A. Müller, *Angew. Chemie Int. Ed. English*, 1991, 30, 34–48.

21 L. C. W. Baker and D. C. Glick, *Chem. Rev.*, 1998, 98, 3–49.

22 A. Werner, *Zeitschrift f*[illegible]*r Anorg. Chemie*, 1893, **3**, 267–330.

23 M. T. Pope, *Inorg. Chem.*, 1972, 11, 1973–1974.

24 W. X. Lipscomb, *Inorg. Chem.*, 1965, **4**, 132–134.

25 A. Müller, E. Krickemeyer, M. Penk, V. Wittneben and J. Döring, *Angew. Chemie Int. Ed. English*, 1990, **29**, 88–90.

26 M. I. Khan, A. Müller, S. Dillinger, H. Bögge, Q. Chen and J. Zubieta, *Angew. Chemie Int. Ed. English*, 1993, **32**, 1780–1782.

27 M. T. POPE, *Inorg. Chem. concepts*, 1983, **8**, XIII-180 p.

28 R. J. Errington, M. D. Kerlogue and D. G. Richards, *Non-Aqueous Routes to a New Polyoxotungstate*, 1993.

29 P. Gouzerh and A. Proust, *Chem. Rev.*, 1998, **98**, 77–111.

30 M. H. Rosnes, C. Yvon, D. L. Long and L. Cronin, *Dalt. Trans.*, 2012, **41**, 10071–10079.

31 S. Spillane, R. Sharma, A. Zavras, R. Mulder, C. A. Ohlin, L. Goerigk, R. A. J. O'Hair and C. Ritchie, *Angew. Chemie - Int. Ed.*, 2017, **56**, 8568–8572.

32 E. Garrido Ribó, N. L. Bell, W. Xuan, J. Luo, D. L. Long, T. Liu and L. Cronin, *J. Am. Chem. Soc.*, 2020, **142**, 17508–17514.

33 A. Michailovski and G. R. Patzke, *Chem. - A Eur. J.*, 2006, **12**, 9122–9134.

34 L. Lisnard, A. Dolbecq, P. Mialane, J. Marrot and F. Sécheresse, *Inorganica Chim. Acta*, 2004, **357**, 845–852.

35 H. N. Miras, D. L. Long and L. Cronin, in *Advances in Inorganic Chemistry*, Academic Press Inc., 2017, vol. 69, pp. 1–28.

36 H. N. Miras, C. Mathis, W. Xuan, D. L. Long, R. Pow and L. Cronin, *Proc. Natl. Acad. Sci. U. S. A.*, 2020, **117**, 10699–10705.

37 W. Clegg, G. M. Sheldrick, C. D. Garner and I. B. Walton, *Acta Crystallogr. Sect. B Struct. Crystallogr. Cryst. Chem.*, 1982, **38**, 2906–2909.

38 C. D. Garner, N. C. Howlader, F. E. Mabbs, A. T. McPhail, R. W. Miller and K. D. Onan, *J. Chem. Soc. Dalt. Trans.*, 1978, 1582–1589.

39 J. Fuchs, W. Freiwald and H. Hartl, *Acta Crystallogr. Sect. B Struct. Crystallogr. Cryst. Chem.*, 1978, **34**, 1764–1770.

40 P. Müscher-Polzin, C. Näther and W. Bensch, *Zeitschrift fur Naturforsch. - Sect. B J. Chem. Sci.*, 2020, **75**, 233–237.

41 F. Pickhard and H. Hartl, *Zeitschrift f*[illegible]*r Anorg. und Allg. Chemie*, 1997, **623**, 1311–1316.

42 S. Yerra, S. R. Amanchi and S. K. Das, *J. Mol. Struct.*, 2014, **1062**, 53–60.

43 S. Himeno, M. Takamoto, M. Hoshiba, A. Higuchi and M. Hashimoto, *Bull. Chem. Soc. Jpn.*, 2004, **77**, 519–524.

44 K. Y. Matsumoto, A. Kobayashi and Y. Sasaki, *Bull. Chem. Soc. Jpn.*, 1975, **48**, 3146–3151.

45 A. Tézé, J. Canny, L. Gurban, R. Thouvenot and G. Hervé, *Inorg. Chem.*, 1996, **35**, 1001–1005.

46 J. Rowsell and L. F. Nazar, , DOI:10.1021/ja993711.

47 P. Mialane, A. Dolbecq, L. Lisnard, A. Mallard, J. Marrot and F. Sécheresse, *Angew. Chemie - Int. Ed.*, 2002, **41**, 2398–2401.

48 G. Johansson, L.-O. Gullman, A. Kjekshus and R. Söderquist, *Acta Chem. Scand.*, 1960, **14**, 771–773.

49 O. Sadeghi, L. N. Zakharov and M. Nyman, *Science (80-.).*, 2015, **347**, 1359 LP – 1362.

50 H. Wang, S. Hamanaka, Y. Nishimoto, S. Irle, T. Yokoyama, H. Yoshikawa and K. Awaga, *J. Am. Chem. Soc.*, 2012, **134**, 4918–4924.

51 X. X. Han, Y. F. He, C. Te Hung, L. L. Liu, S. J. Huang and S. Bin Liu, *Chem. Eng. Sci.*, 2013, **104**, 64–72.

52 N. Mizuno and M. Misono, *Chem. Rev.*, 1998, **98**, 199–217.

53 H. T. Evans, *J. Am. Chem. Soc.*, 1948, **70**, 1291–1292.

54 A. Perloff, *Inorg. Chem.*, 1970, **9**, 2228–2239.

55 C. Martin, C. Lamonier, M. Fournier, O. Mentré, V. Harlé, D. Guillaume and E. Payen, *Inorg. Chem.*, 2004, **43**, 4636–4644.

56 B. Dawson, *Acta Crystallogr.*, 1953, **6**, 113–126.

57 F.-Q. Zhang, W. Guan, L.-K. Yan, Y.-T. Zhang, M.-T. Xu, E. Hayfron-Benjamin and Z.-M. Su, *Inorg. Chem.*, 2011, **50**, 4967–4977.

58 L. Vilà-Nadal, S. Romo, X. López and J. M. Poblet, Springer, Dordrecht, 2012, pp. 171–183.

59 D. K. Lyon and R. G. Finke, *Inorg. Chem.*, 1990, 29, 1787–1789.

60 L. E. Briand, G. T. Baronetti and H. J. Thomas, *Appl. Catal. A Gen.*, 2003, **256**, 37–50.

61 L. C. W. Baker, G. A. Gallagher and T. P. McCutcheon, *J. Am. Chem. Soc.*, 1953, **75**, 2493–2495.

62 W. P. Griffith, N. Morley-Smith, H. I. S. Nogueira, A. G. F. Shoair, M. Suriaatmaja, A. J. P. White and D. J. Williams, *J. Organomet. Chem.*, 2000, **607**, 146–155.

63 S. Eliska, A. Harchani, M. M. Ftini, M. Dusek and A. Haddad, *Acta Crystallogr. Sect. C Struct. Chem.*, 2020, **76**, 164–169.

64 V. Shivaiah, T. Arumuganathan and S. K. Das, *Inorg. Chem. Commun.*, 2004, **7**, 367–369.

65 I. Nagazi and A. Haddad, *J. Clust. Sci.*, 2014, **25**, 627–638.

66 D. D. Dexter and J. V. Silverton, *J. Am. Chem. Soc.*, 1968, **90**, 3589–3590.

67 J. L. T. Waugh, D. P. Shoemaker and L. Pauling, *Acta Crystallogr.*, 1954, **7**, 438–441.

68 H. Tan, Y. Li, W. Chen, D. Liu, Z. Su, Y. Lu and E. Wang, *Chem. - A Eur. J.*, 2009, **15**, 10940–10947.

69 A. Müller, E. Krickemeyer, H. Bögge, M. Schmidtmann, C. Beugholt, P. Kögerler and C. Lu, *Angew. Chemie Int. Ed.*, 1998, **37**, 1220–1223.

70 A. Müller, S. Q. N. Shah, H. Bögge and M. Schmidtmann, *Nature*, 1999, **397**, 48–50.

71 A. Müller, B. Botar, S. K. Das, H. Bögge, M. Schmidtmann and A. Merca,

Polyhedron, 2004, **23**, 2381–2385.

72 L. Vilà-Nadal, A. Rodríguez-Fortea, L.-K. Yan, E. F. Wilson, L. Cronin and J. M. Poblet, *Angew. Chemie Int. Ed.*, 2009, **48**, 5452–5456.

73 A. J. Bissette and S. P. Fletcher, *Angew. Chemie Int. Ed.*, 2013, **52**, 12800–12826.

74 R. Plasson, A. Brandenburg, L. Jullien and H. Bersini, *J. Phys. Chem. A*, 2011, **115**, 8073–8085.

75 E. V. Skorb and S. N. Semenov, *Life*, 2019, **9**, 1–10.

76 T. Bánsági and A. F. Taylor, *Tetrahedron*, 2017, **73**, 5018–5022.

77 F. A. Chandra, G. Buzi and J. C. Doyle, *Proc. Am. Control Conf.*, 2009, 319–324.

78 W. Hordijk, J. Hein and M. Steel, *Entropy*, 2010, **12**, 1733–1742.

79 W. Hordijk, *Bioscience*, 2013, **63**, 877–881.

80 G. Panzarasa, T. Sai, A. L. Torzynski, K. Smith-Mannschott and E. R. Dufresne, *Mol. Syst. Des. Eng.*, 2020, **5**, 445–448.

81 R. Breslow, *Tetrahedron Lett.*, 1959, **1**, 22–26.

82 H. J. Cleaves, in *Encyclopedia of Astrobiology*, Springer Berlin Heidelberg, 2011, pp. 600–605.

83 E. Bagherzadeh, S. M. Zebarjad, H. R. Madaah Hosseini and P. Chagnon, *CrystEngComm*, 2019, **21**, 544–553.

84 M. G. Goesten, M. F. De Lange, A. I. Olivos-Suarez, A. V Bavykina, P. Serra-Crespo, C. Krywka, F. M. Bickelhaupt, F. Kapteijn and J. Gascon, *Nat. Commun.*, , DOI:10.1038/ncomms11832.

85 H. N. Miras, J. Yan, D.-L. Long and L. Cronin, *Chem. Soc. Rev. Chem. Soc. Rev*, 2012, **41**, 7403–7430.

86 C. Schäffer, A. M. Todea, H. Bögge, E. Cadot, P. Gouzerh, S. Kopilevich, I. A. Weinstock and A. Müller, *Angew. Chemie Int. Ed.*, 2011, **50**, 12326–12329.

87 H. Y. Zang, J. W. Purcell, D. L. Long, H. N. Miras and L. Cronin, *Chem. Commun.*, 2017, **53**, 8585–8587.

88 F. Bannani, bastien Floquet, N. Leclerc-Laronze, M. Haouas, F. Taulelle, me Marrot, P. Ko and E. Cadot, *J. Am. Chem. Soc*, 2012, **134**, 8.

89 H. N. Miras, L. Vilà-Nadal and L. Cronin, *Chem. Soc. Rev.*, 2014, **43**, 5679–5699.

90 C. W. Craig, L. Hill, Goodrich, *Chem. Rev.*, 1998, **98**, 1–2.

91 J. F. Keggin, *Nature*, 1933, 131, 908–909.

92 R. Al-Oweini, B. S. Bassil, M. Itani, D. B. Emiroğlu and U. Kortz, *Acta Crystallogr. Sect. C*, 2018, **74**, 1390–1394.

93 M. Barsukova-Stuckart, N. V. Izarova, R. Barrett, Z. Wang, J. van Tol, H. W. Kroto, N. S. Dalal, B. Keita, D. Heller and U. Kortz, *Chem. A Eur. J.*, 2012, **18**, 6167–6171.

94 R. Al-Oweini, A. Sartorel, B. S. Bassil, M. Natali, S. Berardi, F. Scandola, U. Kortz and M. Bonchio, *Angew. Chem. Int. Ed.*, 2014, **53**, 11182–11185.

95 S. G. Mitchell, P. I. Molina, S. Khanra, H. N. Miras, A. Prescimone, G. J. T. Cooper, R. S. Winter, E. K. Brechin, D. L. Long, R. J. Cogdell and L. Cronin, *Angew. Chemie - Int. Ed.*, 2011, **50**, 9154–9157.

96 P. I. Molina, H. N. Miras, D.-L. Long and L. Cronin, *Dalton Trans.*, 2014, **43**, 5190–9.

97 D. L. Long, R. Tsunashima and L. Cronin, *Angew. Chemie - Int. Ed.*, 2010, **49**, 1736–1758.

98 J. M. Cameron, L. Vilà-Nadal, R. S. Winter, F. Iijima, J. C. Murillo, A. Rodríguez-Fortea, H. Oshio, J. M. Poblet and L. Cronin, *J. Am. Chem. Soc.*, 2016, **138**, 8765–

8773.

99 H. N. Miras, E. F. Wilson and L. Cronin, *Chem. Commun.*, 2009, 1297–1311.

100 M. J. Deery, O. W. Howarth and K. R. Jennings, *J. Chem. Soc. - Dalt. Trans.*, 1997, 4783–4788.

101 C. A. Ohlin, *Chem. - An Asian J.*, 2012, 7, 262–270.

102 L. Vilà-Nadal, E. F. Wilson, H. N. Miras, A. Rodríguez-Fortea, L. Cronin and J. M. Poblet, *Inorg. Chem.*, 2011, **50**, 7811–7819.

103 I. Nakamura, H. N. Miras, A. Fujiwara, M. Fujibayashi, Y.-F. Song, L. Cronin and R. Tsunashima, *J. Am. Chem. Soc.*, , DOI:10.1021/ja512758j.

104 F. Xu, R. A. Scullion, J. Yan, H. N. Miras, C. Busche, A. Scandurra, B. Pignataro, D. L. Long and L. Cronin, *J. Am. Chem. Soc.*, 2011, **133**, 4684–4686.

105 H. N. Miras, H. Y. Zang, D. L. Long and L. Cronin, *Eur. J. Inorg. Chem.*, 2011, 5105–5111.

106 L. V. Nadal, A. Rodríguez-Fortea, L. K. Yan, E. F. Wilson, L. Cronin and J. M. Poblet, *Angew. Chemie - Int. Ed.*, 2009, **48**, 5452–5456.

107 R. E. Schreiber, L. Houben, S. G. Wolf, G. Leitus, Z. L. Lang, J. J. Carbó, J. M. Poblet and R. Neumann, *Nat. Chem.*, 2017, **9**, 369–373.

108 X. López, J. J. Carbó, C. Bo and J. M. Poblet, *Chem. Soc. Rev.*, 2012, **41**, 7537–7571.

109 D. Sures, M. Segado, C. Bo and M. Nyman, *J. Am. Chem. Soc.*, 2018, **140**, 10803–10813.

110 H. N. Miras, C. Mathis, W. Xuan, D. L. Long, R. Pow and L. Cronin, *Proc. Natl. Acad. Sci. U. S. A.*, 2020, **117**, 10699–10705.

111 D. Sievers and G. von Kiedrowski, *Nature*, 1994, **369**, 221–224.

112 D. H. Lee, J. R. Granja, J. A. Martinez, K. Severin and M. R. Ghadiri, *A self-replicating peptide*, 1996, vol. 382.

113 E. Kassianidis and D. Philp, *Angew. Chem.Int .ed.*, 2006, **45**, 6344–6348.

114 J. W. Sadownik and D. Philp, *Angew. Chemie - Int. Ed.*, 2008, **47**, 9965–9970.

115 J. M. Quayle, A. M. Z. Slawin and D. Philp, *Tetrahedron Lett.*, 2002, **43**, 7229–7233.

116 A. Vidonne and D. Philp, *European J. Org. Chem.*, 2009, 593–610.

117 A. J. Bissette and S. P. Fletcher, *Angew. Chemie Int. Ed.*, 2013, **52**, 12800–12826.

118 D. S. Salley, G. A. Keenan, D. L. Long, N. L. Bell and L. Cronin, *ACS Cent. Sci.*, 2020, **6**, 1587–1593.